Mono- and Bimetallic Bipyridyl Polyene Complexes Containing 17-Electron Molybdenum Mononitrosyl Centers: Electrochemical, Spectroscopic, and Magnetic Studies

Sean L. W. McWhinnie,[†,‡] James A. Thomas,[†] Thomas A. Hamor,[†] Christopher J. Jones,*[,†] Jon A. McCleverty,*[,§] David Collison,[||] Frank E. Mabbs,[||] Charlie J. Harding,[⊥] Lesley J. Yellowlees,[▽] and Michael G. Hutchings[#]

School of Chemistry, The University of Birmingham, Edgbaston, Birmingham B15 2TT, U.K., School of Chemistry, University of Bristol, Cantock's Close, Bristol BS8 1TS, U.K., Department of Chemistry, University of Manchester, Manchester M13 9PL, U.K., Department of Chemistry, The Open University, Walton Hall, Milton Keynes MK7 6AA, U.K., Department of Chemistry, The University of Edinburgh, Kings Buildings, West Mains Road, Edinburgh EH9 3JJ, U.K., and Zeneca Specialties Research Centre, Blackley, Manchester M9 8ZS, U.K.

Received March 24, 1995[⊗]

The monometallic bipyridyl complexes [MoTp*(NO)X(L-L)] [Tp* = $HB(3,5\text{-}Me_2C_3HN_2)_3$; L-L = 3,3′-bipyridine, 4,4′-bipyridine, 1,2-bis(4-pyridyl)ethane and X = Cl; L-L = 4,4′-$NC_5H_4(CH{=}CH)_nH_4C_5N$, n = 0, 1, 2, 3, 4 (all *trans*) and X = Cl, I] and their bimetallic counterparts [{(NO)MoTp*X}$_2$(L-L)] have been synthesized, together with [MoTp*(NO)Cl{4-$NC_5H_4CH{=}CHC(Me){=}CHCH{=}$}]$_2$. The single crystal X-ray structure of [{MoTp*-(NO)Cl}$_2${4,4′-$NC_5H_4(CH{=}CH)_4H_4C_5N$}] confirms that the polyene chain is in the all-*trans* configuration and exhibits normal bond length alternation with [$r_{C-C}-r_{C=C}$] = 0.092 Å. The Mo−Mo distance is 20.764(3) Å, and the Mo−N(pyridyl) bond distance of 2.196(6) Å indicates a much lower degree of Mo−(N)ligand π bonding than that found in related amide complexes where Mo−N(amide) distances are typically some 0.3 Å shorter. Cyclic voltammograms of the monometallic complexes contain a single one-electron reduction process, whereas those of the bimetallic complexes contain two one-electron processes. The separation between the two reduction potentials varies almost linearly with polyene chain length from the statistical limit of 36 mV in the bipyridyl dimethyldecapentene derivative to 765 mV in the 4,4′-bipyridyl derivative. The isovalent bimetallic complexes exhibit EPR signals (300 K) which show hyperfine coupling to two equivalent metal centers with $J \gg A$ and are consistent with the unpaired electrons occupying orbitals which are predominantly metal in character. Magnetic measurements indicate the presence of an antiferromagnetic interaction in [{MoTp*(NO)Cl}$_2${4,4′-NC_5H_4-$(CH{=}CH)_4H_4C_5N$}] with a coupling $-2J$ estimated to be *ca.* 80 cm^{-1} over a distance of *ca.* 2 nm.

Introduction

The search for new molecular materials with potential applications in molecular electronic or electrooptic devices has aroused renewed interest in studies of transition metal complexes.[1] In particular, heterobimetallic and mixed valence[2,3] complexes are proving to be a rich source of new metal−organic materials which exhibit important bulk properties such as nonlinear optical[4] (NLO) phenomena or ferrimagnetism.[5] In many cases an important feature of the molecular design is the use of redox active metal centers as potential electron donor or acceptor sites within a polarizable molecular framework. The finding that doped *trans*-polyacetylene exhibits substantial third-order nonlinear optic properties[6] suggests the possibility that combining redox active transition metal centers with polyene-containing ligands might lead to new molecular materials with enhanced NLO properties.[7] This possibility prompted us to investigate a series of complexes in which two redox active metal centers are linked by a bridging ligand containing a polyene link. The ability of polyenes to support metal−metal interactions has been demonstrated previously in bimetallic complexes containing pentammine ruthenium termini linked by

[†] The University of Birmingham.
[‡] Present address: Department of Chemistry, Brunel University, Uxbridge, Middlesex UB8 3PH, U.K.
[§] University of Bristol.
[||] University of Manchester.
[⊥] The Open University.
[▽] The University of Edinburgh.
[#] Zeneca Specialties Research Centre.
[⊗] Abstract published in *Advance ACS Abstracts,* December 15, 1995.

(1) *Inorganic Materials*; Bruce, D. W., O'Hare, D., Eds.; Wiley, Chichester, U.K., 1992.
(2) (a) Robin, M. B.; Day, P. *Adv. Inorg. Chem. Radiochem.* **1967**, *10*, 247−422. (b) Allen, G. C.; Hush, N. S. *Prog. Inorg Chem.* **1967**, *8*, 357−390. (c) Hush, N. S. *Prog. Inorg Chem.* **1967**, *8*, 391−444. (d) Meyer, T. J. *Prog. Inorg. Chem.* **1983**, *30*, 389−440. (e) Clark, R. J. H. *Chem. Soc. Rev.* **1984**, *13*, 219−244. (f) Meyer, T. J.; Taube, H. In *Comprehensive Coordination Chemistry;* Wilkinson, G., Gillard, R. D., McCleverty, J. A., Eds.; Pergamon: Oxford, U.K., 1987; Vol. 1, Chapter 7.2, pp 331−384.
(3) Creutz, C. *Prog. Inorg. Chem.* **1983**, *30*, 1−73.
(4) (a) Marder, S. R. in ref 1. (b) Green, M. L. H.; Marder, S. R.; Thompson, M. E.; Bandy, J. A.; Bloor, D.; Kolinsky, P. V.; Jones, R. J. *Nature* **1987**, *330*, 360−362. (c) Coe, B. J.; Jones, C. J.; McCleverty, J. A.; Bloor, D.; Kolinsky, P. V.; Jones, R. J. *J. Chem. Soc., Chem Commun.* **1990**, 940−943.
(5) (a) Stumpf, H. O.; Ouahab, L.; Pei, Y.; Grandjean, D.; Kahn, O. *Science* **1993**, *261*, 447−449. (b) Miller, J. S.; Epstein, A. J.; Rieff, W. M. *Chem. Rev.* **1988**, *88*, 201−220.
(6) Prasad, P. N.; Williams, D. J. *Introduction to Non-Linear Optical Effects in Molecules and Polymers;* Wiley: New York, 1991; Chapter 10, p 238.
(7) (a) Lehn, J.-M. In *Non-Linear Optical Properties of Organic Molecules and crystals;* Chemla, D. S., Zyss, J., Eds.; Academic Press: New York, 1987; Vol. 2, p 215−220. (b) Effenburger, F.; Schloser, H.; Bauerle, P.; Maier, S.; Port, H.; Wolf, H. C. *Angew. Chem., Int. Ed. Engl.* **1988**, *27*, 281−284. (c) Gust, D.; Moore, T. A.; Moore, A. L.; Barrett, D.; Harding, L. O.; Makings, L. R.; Liddell, P. A.; DeShryver, F. C.; Van der Auweraer, M.; Bensasson, R. V.; Rougee, M. *J. Am. Chem. Soc.* **1988**, *110*, 321−323. (d) Gust, D.; Moore, T. A.; Moore, A. L.; Lee, S.-J.; Bittersman, E.; Luttrull, D. K.; Rehms, A. A.; DeGraziano, J. M.; Ma, X. C.; Gao, F.; Belford, R. E.; Trier, T. T. *Science* **1990**, *248*, 199−201.

0020-1669/96/1335-0760$12.00/0

α,ω-bipyridyl polyene bridging ligands.[8] Here we report our findings on complexes containing 17-electron molybdenum mononitrosyl centers.

In homobimetallic complexes containing entirely metal-based redox centers, an estimate of the metal−metal interaction may be obtained from the value of the comproportionation constant, K_c, for the comproportionation equilibrium (1)

$$[[M^*(L\text{-}L)M^*]^{(z-1)}] + [[M^*(L\text{-}L)M^*]^{(z+1)}] = 2[[M^*(L\text{-}L)M^*]^{(z)}] \quad (1)$$

where $[M^*(L\text{-}L)M^*]^{(z)}$ represents a mixed valence bimetallic complex containing two metal centers M* separated by a bridging ligand L-L and having an overall charge *z*.

In principle electrochemical measurements provide a simple means of determining K_c, since an oxidized isovalent bimetallic complex should exhibit two one-electron reduction processes at potentials $E_f(1)$ and $E_f(2)$ separated by a potential difference, ΔE_f, which is related to K_c by the expression $\log K_c = \Delta E_f/59$ mV.[9] However, the relatively low resolution of electrochemical techniques such as cyclic voltammetry means that accurate determinations of K_c values less than *ca*. 500 (corresponding with a ΔE_f value of *ca*. 160 mV) are difficult.[10] In many of the complexes studied so far, K_c values of less than 500 are involved. The K_c values of the bimetallic pentammine ruthenium complexes containing α,ω-bipyridyl polyene bridging ligands, for example, were found to be in the range 4−20 and were determined using electronic spectroscopy.[8] The use of transition metal based couples other than $\{Ru(NH_3)_5\}^{2+/3+}$ can give compounds which exhibit much larger electrochemical effects.[11] Thus, while the isovalent complex $[\{Ru(NH_3)_5\}_2(4,4'\text{-}NC_5H_4C_5H_4N)]^{4+}$ exhibits two oxidation waves separated by 75 mV,[12] a ΔE_f value of 765 mV has been obtained from the corresponding molybdenum mononitrosyl derivative, $[\{MoTp^*(NO)Cl\}_2(4,4'\text{-}NC_5H_4C_5H_4N)]$.[13] In principle this large ΔE_f value might provide a basis for determining the variation in K_c with increasing polyene chain length through a series of bipyridyl polyene bridged bimetallic complexes. Accordingly we have synthesized the compounds $[\{MoTp^*(NO)X\}_x(L\text{-}L)]$ {L-L = $4,4'\text{-}NC_5H_4(CH{=}CH)_nC_5H_4N$ (n = 0, 1, 2, 3, 4), X = Cl, I, x = 1, 2; L-L = $\{NC_5H_4\text{-}4\text{-}CH{=}CHC(Me){=}CHCH{=}\}_2$, X = Cl, x = 2} Figures 1 and 2) and examined their electrochemical properties.[14] The related complexes with X = Cl and L-L = $3,3'\text{-}NC_5H_4C_5H_4N$ (3,3′-bpy) or $4,4'\text{-}NC_5H_4CH_2CH_2C_5H_4N$ (bpa) were also synthesized to determine the consequences of removing any mesomeric interactions between the pyridyl nitrogen donor sites. The X-ray crystal structure of $[\{MoTp^*(NO)Cl\}_2(4,4'\text{-}NC_5H_4(CH{=}CH)_4C_5H_4N)]$ was also obtained to determine the Mo−Mo distance, the degree of bond alternation in the polyene chain, and the torsion angles within it.

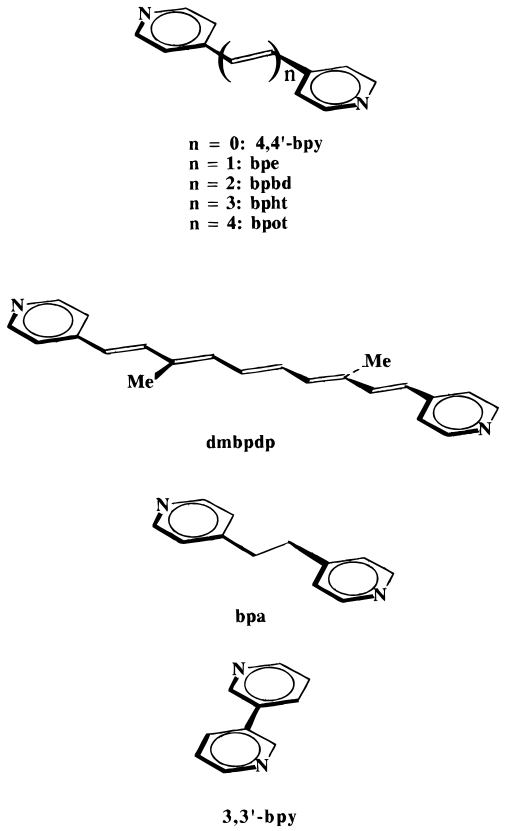

Figure 1. Structural formulas of the ligands used in this work.

Experimental Section

General Details. All chemicals obtained from commercial sources were used without further purification unless otherwise stated. $[MoTp^*(NO)X_2]$ (X is Cl or I)[15] and the bipyridyl polyenes bpbd, bpht, bpot, and dmbpdp were synthesized using published methods.[8a,16] All reaction solvents were dried and further purified where necessary, according to standard literature methods. When used with Schlenk apparatus, solvents were vacuum degassed before reactants were introduced. All reactions were carried out under nitrogen using Schlenk apparatus unless otherwise stated. Column chromatography was carried out in glass columns fitted with no. 2 or no. 3 glass sinters with silica gel as the stationary phase. Thin layer chromatography was carried out on Merck aluminum sheets coated with silica gel 60−200 mesh to a thickness of 0.2 mm. Products were initially identified as mono- or bimetallic complexes from their mass spectra and R_f values. Microanalyses for carbon, hydrogen, and nitrogen were provided by the Microanalytical Service of the School of Chemistry at Birmingham University.

Infrared spectra were obtained from KBr disks using a Perkin-Elmer 297 instrument. Mass spectra were run on a Kratos MS80RF instrument. EI spectra were run using a 50−70 eV ionization potential, and FAB spectra were run using an 8 kV argon gun, samples being mounted in a NOBA matrix unless otherwise stated. EPR spectra were obtained using a Varian E112 spectrometer. Frozen solution spectra were obtained with the use of an Oxford Instruments ESR9 cyrostat. Samples were dissolved in a dichloromethane/toluene mixture as the solvent. Magnetic susceptibility measurements were made with an Oxford Instruments resistive Faraday balance. Molar susceptibilities were corrected for the diamagnetic contribution of ligands using Pascal's constants. Cyclic voltammetry was carried out using a PAR 360 potentiostat with built-in wave form generator and the Condecon 310

(8) (a) Woitellier, S.; Launay, J. P.; Spangler, C. W. *Inorg. Chem.* **1989**, *28*, 758−762. (b) Reimers, J. R.; Hush, N. S. *Inorg. Chem.* **1990**, *29*, 4510−4513.
(9) Richardson, D. E.; Taube, H. *Inorg. Chem.* **1981**, *20*, 1278−1285.
(10) Sutton, J. E.; Sutton, P.; Taube, H. *Inorg. Chem.* **1979**, *18*, 1017−1021.
(11) Bruns, W.; Kaim, W. In *Mixed Valency Systems: Applications in Chemistry, Physics, Biology;* Prassides, K., Ed.; Kluwer Academic Publishers: Dordrecht, The Netherlands, 1991; pp 365−370.
(12) Sutton, J. E.; Taube, H. *Inorg. Chem.* **1981**, *20*, 3125−3134.
(13) McWhinnie, S. L. W.; Jones, C. J.; McCleverty, J. A.; Collison, D.; Mabbs, F. E. *J. Chem. Soc., Chem Commun.* **1990**, 940−943.
(14) Thomas, J. A.; Jones, C. J.; McCleverty, J. A.; Collison, D.; Mabbs, F. E.; Harding C. J.; Hutchings, M. G. *J. Chem. Soc., Chem Commun.* **1992**, 1796−1798.
(15) (a) Trofimenko, S. *Inorg. Chem.* **1969**, *8*, 2675−2680. (b) Reynolds, S. J.; Smith, C. F.; Jones, C. J.; McCleverty, J. A. *Inorg. Synth.* **1985**, *23*, 4−9.
(16) (a) Carsky, P.; Hunig, S.; Stemmler, I.; Scheutzow, D. *Liebigs Ann. Chem.* **1980**, 291−304. (b) Arrhenius, T. S.; Blanchard-Desce, M.; Dvolaitzky, M.; Lehn, J.-M.; Malthete, J. *Proc. Natl. Acad. Sci. U.S.A.* **1986**, *83*, 5355−5359.

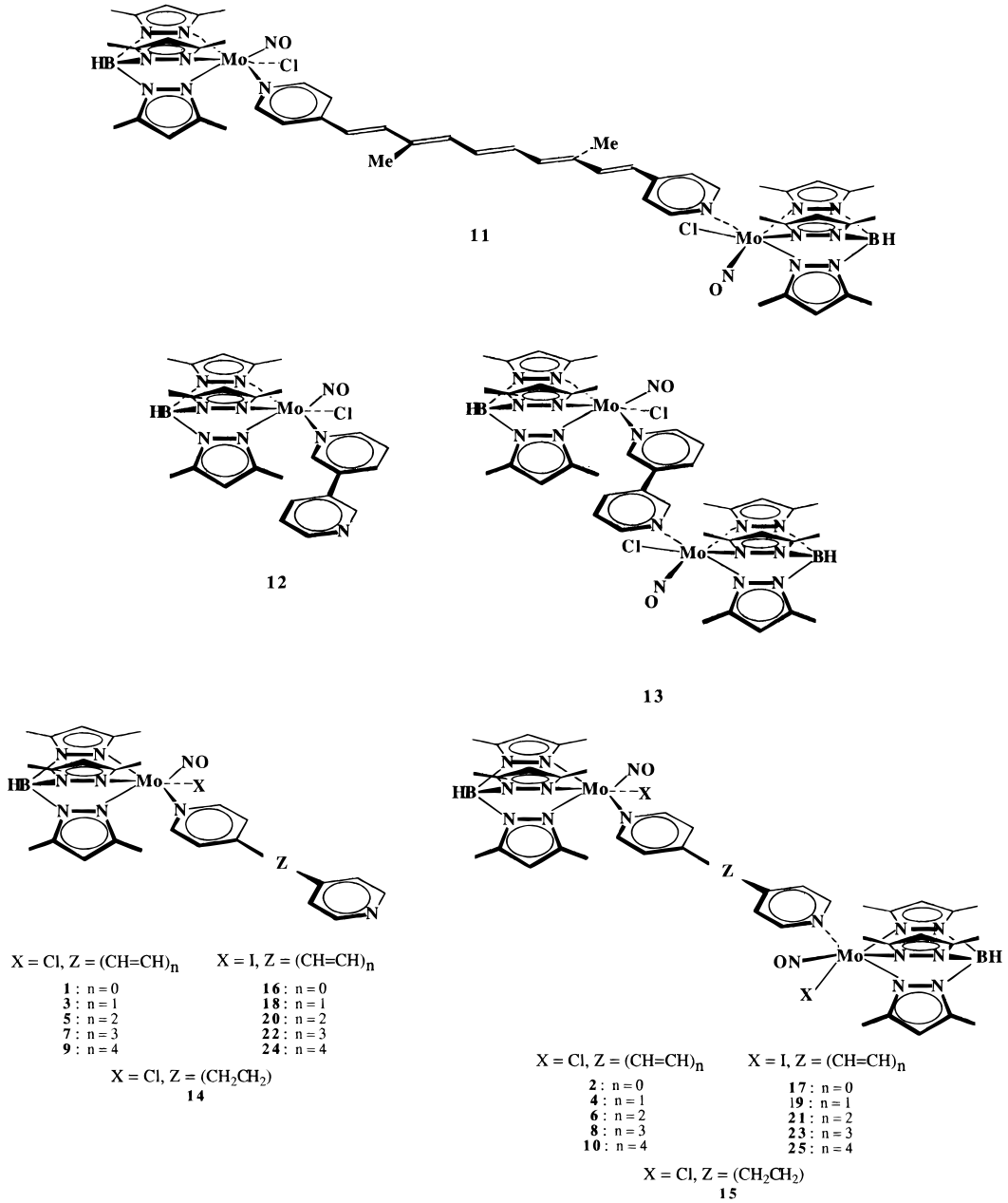

Figure 2. Structural formulas of the new complexes prepared in this work.

system, which allows data collection and processing to be computer assisted. Measurements were made using 2×10^{-3} mol dm^{-3} solutions in dry solvents under a nitrogen atmosphere, with 0.2 mol dm^{-3} [Bu_4N][BF_4] as the supporting electrolyte. A platinum bead electrode was used in all cases, and potentials were measured vs a saturated calomel reference electrode with ferrocene added as an internal standard. Ultraviolet−visible spectra were obtained using a Shimadzu UV-240 spectrometer. Samples were recorded using a matched cell containing solvent in order to correct for background effects. Spectroelectrochemical measurements were made using a Perkin-Elmer Lambda 9 spectrometer while samples were electrolyzed in an OTTLE cell using a Metrohm potentiostat.

Synthetic procedures. (a) Preparation of [MoTp*(NO)Cl(4,4′-bpy)] (1) and [{MoTp*(NO)Cl}$_2$(μ-4,4′-bpy)] (2). A mixture of [Et_3NH][MoTp*(NO)Cl_2] (200 mg, 0.34 mmol) and 4,4′-bipyridyl (23.4 mg, 0.15 mmol) was heated under reflux in toluene (10 cm^3) for 2 h during which time the solution became dark blue in color. The mixture was cooled, filtered, and evaporated to dryness. The reaction products in the residue were separated by column chromatography (30 × 2 cm, silica gel, eluent 98.5/1.5 CH_2Cl_2/THF for the first three fractions, 98/2 CH_2Cl_2/THF thereafter). Four fractions were obtained; the first yellow and second green fraction were discarded. The dark blue third fraction was identified as [{MoTp*(NO)Cl}$_2$(μ-4,4′-bpy)] (53.5 mg, 30%) and the fourth cherry red fraction as [MoTp*(NO)Cl(4,4′-bpy)] (11.2 mg, 5%).

(b) Preparation of [MoTp*(NO)Cl(bpe)] (3) and [{MoTp*(NO)Cl}$_2$(μ-bpe)] (4). [Et_3NH][MoTp*(NO)Cl_2] (290 mg, 0.49 mmol) and 1,2-bis(4-pyridyl)ethylene (41 mg, 0.22 mmol) were heated under reflux in toluene (15 cm^3) for 2 h. The solution was cooled, filtered, and evaporated to dryness. Column chromatography was carried out as for **1** and **2**; the first red and second gray fractions were discarded, but the green third fraction was identified as [{MoTp*(NO)Cl}$_2$(μ-bpe)] (53.3 mg, 29%) and the red fourth fraction as [MoTp*(NO)Cl(bpe)] (24.0 mg, 11%).

(c) Preparation of [MoTp*(NO)Cl(bpbd)] (5) and [{MoTp*(NO)Cl}$_2$(μ-bpbd)] (6). Triethylamine (0.5 cm^3) was added to toluene (50 cm^3) containing bipyridyl butadiene (104 mg, 0.5 mmol) and [MoTp*(NO)Cl_2] (494 mg, 1 mmol); the mixture was heated under reflux for 15 h and filtered, and both the residue and filtrate were retained. The residue was dissolved in dichloromethane, and column chromatography with 99/1 CH_2Cl_2/THF as the eluent afforded a purple fraction which was collected and identified as [{MoTp*(NO)Cl}$_2$(μ-bpbd)] (274 mg, 49%). The filtrate was evaporated to dryness *in vacuo*. The brown solid obtained was redissolved in dichloromethane, and column

chromatography with a 95/5 CH_2Cl_2/THF eluent afforded a red/brown fraction identified as [MoTp*(NO)Cl(bpbd)] (60 mg, 18% with respect to the bpbd ligand).

(d) Preparation of [MoTp*(NO)Cl(bpht)] (7) and [{MoTp*(NO)Cl}$_2$(μ-bpht)] (8). [MoTp*(NO)C1$_2$] was reacted with bpht (117 mg, 0.5 mmol) following the procedure used to synthesize **5** and **6**, yielding [{MoTp*(NO)Cl}$_2$(μ-bpht)] (205 mg, 36%) and [MoTp*(NO)Cl(bpht)] (64 mg, 18%).

(e) Preparation of [MoTp*(NO)Cl(bpot)] (9) and [{MoTp*(NO)Cl}$_2$(μ-bpot)] (10). [MoTp*(NO)C1$_2$] was reacted with bpot (130 mg, 0.5 mmol) following the procedure used to synthesize **5** and **6**, yielding [{MoTp*(NO)Cl}$_2$(μ-bpot)] (217 mg, 37%) and [MoTp*(NO)Cl(bpot)] (95 mg, 26%).

(f) Preparation of [{MoTp*(NO)Cl}$_2$(μ-dmbpdp)] (11). Triethylamine (0.5 cm^3) was added to toluene (60 cm^3) containing bipyridyl dimethyldecapentene (158 mg, 0.5 mmol) and [MoTp*(NO)Cl$_2$] (494 mg, 1 mmol). The mixture was heated under reflux for 15 h after which time the solvent was removed by evaporation *in vacuo*. The solid obtained was dissolved in dichloromethane, and column chromatography with a 98/2 CH_2Cl_2/THF eluent afforded a major orange/brown fraction identified as [{MoTp*(NO)Cl}$_2$(μ-dmbpdp)] {97 mg, 25.0% with respect to [(NO)MoTp*Cl$_2$]}.

(g) Preparation of [MoTp*(NO)Cl(3,3′-bpy)] (12) and [{MoTp*(NO)Cl}$_2$(μ-3,3′-bpy)] (13). [Et$_3$NH][MoTp*(NO)Cl$_2$] (0.5 g, 0.84 mmol) was heated under reflux together with 3,3′-bipyridyl (70 mg, 0.45 mmol) in toluene (40 cm^3) for 4.5 h. The dark red solution was cooled, filtered, and evaporated to dryness. The residue was purified by column chromatography using a 99/1 CH_2Cl_2/THF eluent. The first four fractions were discarded, but the fifth and sixth fractions, which were both red-brown, were collected and identified as, respectively, [{MoTp*(NO)Cl}$_2$(μ-3,3′-bpy)] (72.5 mg, 16%) and [MoTp*(NO)Cl(3,3′-bpy)] (84.8 mg, 16%).

(h) Preparation of [MoTp*(NO)Cl(bpa)] (14) and [{MoTp*(NO)Cl}$_2$(μ-bpa)] (15). [Et$_3$NH][MoTp*(NO)Cl$_2$] (0.50 g, 0.84 mmol) and 1,2-bis(4-pyridyl)ethane (75 mg, 41 mmol) were heated together under reflux in toluene (30 cm^3) for 2 h. The greenish solution was cooled, filtered, and evaporated to dryness. The residue was purified by column chromatography using a 99/1 CH_2Cl_2/THF eluent. The first four fractions were discarded, but the yellow-green fifth and sixth fractions were collected and identified, respectively, as [{MoTp*(NO)Cl}$_2$(μ-bpe)] (75.0 mg, 16%) and [MoTp*(NO)Cl(bpe)] (66.7 mg, 12%).

(i) Preparation of [MoTp*(NO)I(4,4′-bpy)] (16) and [{MoTp*(NO)I}$_2$(μ-4,4′-bpy)] (17). A mixture of triethylamine (0.5 cm^3), 4,4′-bipyridine (78 mg, 0.5 mmol), and [MoTp*(NO)I$_2$] (677 mg, 1 mmol) in toluene (50 cm^3) was heated under reflux for 6 h and was filtered, and the collected residue and filtrate both were retained. The residue was dissolved in dichloromethane, and column chromatography of the solution using a 99/1 CH_2Cl_2/THF eluent afforded a major blue fraction identified as [{MoTp*(NO)I}$_2$(μ-4,4′-bpy)] (170 mg, 27%). The filtrate was reduced in volume by evaporation *in vacuo* until a brown precipitate was produced. This solid was collected and redissolved in the minimum amount of dichloromethane. Column chromatography of this solution using a 95/5 CH_2Cl_2/THF eluent afforded a major red fraction identified as [MoTp*(NO)I(bpy)] (22 mg, 6% based on bpy).

(j) Preparation of [MoTp*(NO)I(bpe)] (18) and [{MoTp*(NO)I}$_2$(bpe)] (19). [MoTp*(NO)I$_2$] was reacted with bpe (91 mg, 0.5 mmol) using the procedure described above for **16** and **17** to give [{MoTp*(NO)I}$_2$(μ-bpe)] (288 mg, 45%) and [MoTp*(NO)I(bpe)] (16 mg, 4.5%).

(k) Preparation of [MoTp*(NO)I(bpbd)] (20) and [{MoTp*(NO)I}$_2$(bpbd)] (21). [MoTp*(NO)I$_2$] was reacted with bpbd (104 mg, 0.5 mmol) using the procedure described above for **16** and **17** to give [{MoTp*(NO)I}$_2$(μ-bpbd)] (308 mg, 47%) and [MoTp*(NO)I(bpbd)] (44 mg, 13%).

(l) Preparation of [MoTp*(NO)I(bpht)] (22) and [{MoTp*(NO)I}$_2$)(μ-bpht)] (23). [MoTp*(NO)I$_2$] was reacted with bpht (117 mg, 0.5 mmol) using the procedure described above for **16** and **17** to give [{MoTp*(NO)I}$_2$(μ-bpht)] (351 mg, 53%) and [MoTp*(NO)I(bpht)] (18 mg, 5%).

(m) Preparation of [MoTp*(NO)I(bpot)] (24) and [{MoTp*(NO)I}$_2$(μ-bpot)] (25). [MoTp*(NO)I$_2$] was reacted with bpot (130 mg, 0.5 mmol) using the procedure described above for **16** and **17** to give [{(NO)MoTp*I}$_2$(μ-bpot)] (297 mg, 45%) and [(NO)MoTp*I(bpot)] (22 mg, 6%).

Table 1. Crystallographic Data for **10** [{Mo(NO)Tp*Cl}$_2$NC$_5$H$_4$(CH$_2$═CH$_2$)$_4$C$_5$H$_4$N]·2CH$_2$Cl$_2$·0.5C$_6$H$_{14}$

formula	$C_{48}H_{60}B_2Cl_2Mo_2N_{16}O_2\cdot 2CH_2Cl_2\cdot 0.5C_6H_{14}$
fw	1390.5
a	18.630(9) Å
b	9.569(6) Å
c	38.574(15) Å
β	98.98(6)°
V	6792 Å^3
Z	4
ρ_{calc}	1.360 g cm^{-3}
space group	$I2/a$ (No. 15)
T	20 °C
λ	0.71069 Å
μ(Mo Kα)	6.40 cm^{-1}
$R(F_o)^a$	0.0648
$R_w(F_o)^b$	0.0939

^{a} $R(F_o) = \sum||F_o| - |F_c||/\sum|F_o|$. ^{b} $R_w(F_o) = [\sum w(F_o - F_c)^2/\sum wF_o^2]^{1/2}$.

Crystal Structure Determination. An irregularly shaped, dark purple crystal of **10**, grown from dichloromethane/hexane, approximate size 0.3 × 0.3 × 0.5 mm, was used in the analysis. Cell dimensions and intensity data were measured on an Enraf-Nonius CAD-4 diffractometer (293 K, Mo Kα X-radiation, graphite monochromator, λ = 0.71069 Å) with $\omega/2\theta$ scans and scan range (ω) = (1.1 + 0.35 tan θ)°. A total of 4335 unique reflections were scanned in the range θ = 2−25° [(h, k, l) = (−20, 0, 0) to (20, 10, 42)]. Three standard reflections remeasured every 2 h showed a slight (*ca.* 7%) diminution of intensity during the period of data collection, and appropriate scaling factors were applied. A total of 3339 structure amplitudes with $F > 5\sigma(F)$ were considered observed and used in the analysis. Crystallographic data are given in Table 1. The structure was determined by Patterson and Fourier methods and refined by least squares, weights $w = 1/[\sigma^2(F) + 0.0003F^2]$, using anisotropic thermal parameters for the non-hydrogen atoms. The carbon atoms of rather ill-defined molecules of dichloromethane and hexane were refined isotropically. The dichloromethane is partially disordered. Hydrogen atoms for the complex were placed in calculated positions riding on their respective bonded atoms with fixed U_{iso} = 0.1 Å^2. Convergence was achieved with all shift/error ratios <0.1, and residual electron density in a final difference map within −0.91 to +0.89 e Å^{-3}. No corrections were made for absorption.

Some difficulty was experienced in locating the positions of the atoms of the nitrosyl group; this was due to a degree of disorder involving the nitrosyl and chloro substituents. Refinement of site occupancies shows that 69(2)% of the molecules have the structure depicted in Figure 3 and 31(2)% have the Cl and NO groups interchanged. The other atoms of the complex exhibit normal vibration parameters and are apparently not affected significantly by the disorder. The minor contributors, Cl1′, N1′, and O1′, were included in the calculations with fixed coordinates, and only their site occupancies and U_{iso} values were refined.

Complex neutral-atom-scattering factors were taken from ref 17. Computations were carried out at the University of Birmingham and Manchester computing centers with the SHELXS-86,[18] SHELX76,[19] and ORTEP[20] programs. Fractional atomic coordinates are listed in Table 2. Full listings of H atom coordinates, bond distances and angles, and anisotropic thermal parameters have been deposited with the Cambridge Crystallographic Data Centre, University Chemical Laboratory, Lensfield Road, Cambridge CB2 1EW, U.K.

(17) *International Tables for X-ray Crystallography*; Kynoch Press: Birmingham, England, 1974; Vol. 4.
(18) Sheldrick, G. M. *Acta Crystallogr.* **1990**, *A46*, 467−473.
(19) Sheldrick, G. M. SHELX76. Program for Crystal Structure Determination. University of Cambridge, England, 1978.
(20) Motherwell, W. D. S.; Clegg, W. PLUTO. Program for Plotting Molecular and Crystal Structures, Cambridge Structural Database System, Users Manual, Part II. Cambridge, England, 1988.

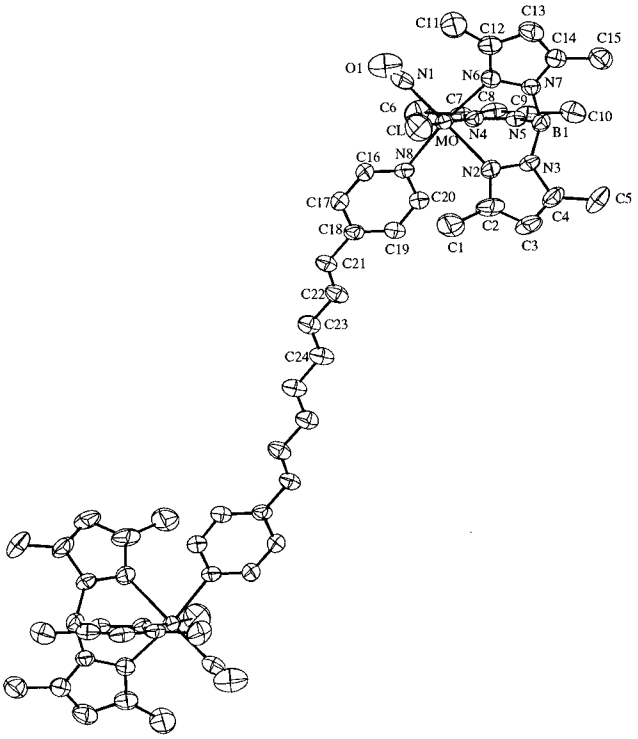

Figure 3. Structure of **10** showing the atom labeling.

Results and Discussion

Synthetic Studies. The recently reported[21] isolation of $[MoTp^*(NO)Cl_2]^-$ and the finding that its reaction with pyridine results in the substitution of only one chloride ligand to give [MoTp*(NO)Cl(py)] together offer a synthetic route to bimetallic complexes, $[\{MoTp^*(NO)Cl\}_2(L\text{-}L)]$, incorporating the bipyridyl bridging ligands (L-L) shown in Figure 1. Generally the reactions between $[MoTp^*(NO)Cl_2]^-$ and L-L afford a mixture of bi- and monometallic complexes which can be separated by column chromatography. Initially these compounds were prepared by the reaction between L-L and $[Et_3NH][MoTp^*(NO)Cl_2]$, separately prepared by reduction of $[MoTp^*(NO)Cl_2]$. However, the bipyridyl polyene complexes were prepared in a single step from $[MoTp^*(NO)Cl_2]$ and the appropriate ligand, L-L, in the presence of NEt_3. The numbering scheme used to identify the complexes and their structures is presented in Figure 2. The reactions with the bipyridyl ligands generally proceeded much more quickly than that with pyridine. However, the yield of [MoTp*(NO)Cl(py)] was higher than that of any of the bipyridyl complexes.

In the syntheses of the bipyridyl polyene complexes it was found that, even with a 1:1 reactant stoichiometry, more bithan monometallic complex was formed and, in the case of dmbpdp, only a bimetallic product could be isolated. The monometallic derivatives were more polar and more soluble than their bimetallic counterparts but were less stable, decomposing over a period of months, whereas the bimetallic complexes could be stored in air for at least a year without significant decomposition. For both series of complexes, solubilities decreased with increasing polyene chain length. Elemental analyses of the bimetallic complexes are in accord with expectation, but three of the monometallic complexes were found to contain dichloromethane as the solvent of crystallization as also indicated by the presence of a group of ions between *m*/*z* 84 and 90 in their mass spectra.

Table 2. Fractional Atomic Coordinates ($\times 10^4$) with Esd's in Parentheses and Equivalent Isotropic Temperature factors ($A^2 \times 10^3$)

	x	*y*	*z*	U_{eq}[a]
Mo(1)	6854(1)	6096(1)	6398(1)	45
Cl(1)	6647(2)	4318(5)	5949(1)	83[b]
N(1)	5986(10)	5655(12)	6573(3)	54[b]
N(2)	7852(4)	6727(7)	6196(2)	52
N(3)	8468(4)	7006(8)	6441(2)	55
N(4)	7181(3)	7681(6)	6800(2)	46
N(5)	7895(4)	7744(6)	6953(2)	47
N(6)	7551(4)	4752(6)	6750(2)	54
N(7)	8235(3)	5219(6)	6888(2)	47
N(8)	6287(3)	7723(7)	6059(2)	47
B(1)	8461(5)	6733(10)	6826(3)	51
O(1)	5460(11)	5540(15)	6661(4)	110[b]
C(1)	7498(7)	6837(16)	5541(3)	100
C(2)	8032(6)	7039(11)	5878(3)	71
C(3)	8743(6)	7498(13)	5919(3)	88
C(4)	9006(5)	7468(10)	6270(3)	73
C(5)	9746(5)	7862(15)	6470(4)	103
C(6)	6034(5)	8882(10)	6864(3)	75
C(7)	6819(5)	8626(8)	6962(2)	50
C(8)	7311(5)	9274(8)	7220(2)	58
C(9)	7971(5)	8705(8)	7206(2)	57
C(10)	8682(6)	9044(10)	7432(3)	78
C(11)	6834(7)	2614(11)	6771(4)	117
C(12)	7490(5)	3456(8)	6861(3)	64
C(13)	8137(6)	3072(9)	7063(3)	71
C(14)	8593(5)	4185(9)	7076(2)	54
C(15)	9362(6)	4337(12)	7250(3)	81
C(16)	5637(4)	7484(9)	5867(2)	54
C(17)	5260(5)	8478(9)	5663(2)	56
C(18)	5537(5)	9820(8)	5642(2)	50
C(19)	6209(5)	10062(9)	5844(2)	53
C(20)	6562(5)	9006(9)	6040(2)	55
C(21)	5129(5)	10865(9)	5423(2)	55
C(22)	5345(5)	12177(9)	5382(2)	57
C(23)	4939(5)	13189(9)	5162(2)	60
C(24)	5201(5)	14485(9)	5114(2)	63
Cl(1′)	5782	5491	6631	91(8)[c]
N(1′)	6700	4769	6063	69(11)[c]
O(1′)	6602	3920	5849	129(22)[c]
Cl(2)	8789(4)	1199(8)	767(3)	287
Cl(3)	8537(6)	3653(11)	1140(3)	307
C(25)	9171(21)	1848(40)	1329(11)	78(11)[d]
C(25A)	8974(18)	1513(30)	1212(9)	52(7)[d]
C(25B)	8499(22)	1940(41)	1176(11)	91(10)[d]
C(26)	6849(12)	4670(24)	−39(6)	70(6)[e]
C(27)	6849(19)	3933(36)	−12(10)	121(11)[e]
C(28)	7188(18)	2242(35)	101(10)	137(11)[e]

[a] $U_{eq} = {}^1/_3$ (trace of the orthogonalized $\mathbf{U}_{ij}$ tensor). [b] Site occupancy 0.69(2). [c] Site occupancy 0.31(2). [d] Site occupancy 0.33. [e] Site occupancy 0.5.

In earlier studies of the reaction between pyridine and the diiodo complex $[MoTp^*(NO)I_2]$ only the bis-substituted product $[MoTp^*(NO)(py)_2]^+$ could be isolated,[22] although the monosubstituted derivatives $[MoTp^*(NO)I(NHC_nH_{2n})]$ ($n = 4, 5$) were isolated with saturated cyclic amines.[23] More recently we have shown[24] that monosubstitution of $[MoTp^*(NO)I_2]$ by unsaturated nitrogen heterocycles occurs in the presence of NEt_3, and a similar procedure was employed to obtain the iodo complexes $[\{MoTp^*(NO)I\}_2(L\text{-}L)]$ (L-L = 4,4′-bpy, bpe, bpbd, bpht, and bpot) and [MoTp*(NO)I(L-L)] for comparison with their chloro counterparts.

(21) McWhinnie, S. L. W.; Jones, C. J.; McCleverty, J. A.; Collison, D.; Mabbs, F. E. *Polyhedron* **1992**, *11*, 2639−2643.

(22) AlObaidi, N.; Edwards, A. J.; Jones, C. J.; McCleverty, J. A.; Neaves, B. D.; Mabbs, F. E.; Collison, D. *J. Chem. Soc., Dalton Trans.* **1989**, 127−132.

(23) AlObaidi, N.; Hamor, T. A.; Jones, C. J.; McCleverty, J. A.; Paxton, K.; Howes, A. J.; Hursthouse, M. B. *Polyhedron* **1988**, *7*, 1931−1938.

(24) McQuillan, F. S.; Green, T.; Hamor, T. A.; Jones, C. J.; Maher, J. P.; McCleverty, J. A. *J. Chem. Soc., Dalton Trans.* **1995**, 3243−3250.

IR Spectra. The IR spectra of the new complexes are very similar, and all contain absorptions attributable to the Tp* ligand, including ν_{max}(BH) at *ca*. 2500 cm^{-1}, ν_{max}(CH) at *ca.* 2920 cm^{-1}, and ν_{max}(C−CH_3) in the range 1365−1445 cm^{-1}. In all cases, ν_{max}(NO) is observed at *ca*. 1600 cm^{-1} in accord with the presence of the reduced 17-electron {MoTp*(NO)} center.[22,25] In addition, ν_{max}(C═C) is observed at *ca*. 1540 cm^{-1}. The IR spectra of the iodo complexes were similar to those of their chloro counterparts. However, in all cases, values for ν_{max}(NO) were around 10−15 cm^{-1} higher, indicating that the electron density at the molybdenum center is lower than that in the chloro complexes.

Mass Spectra. FAB mass spectra of the new compounds contained the expected molecular ions which, because of the isotope distributions of the various elements in the complexes, took the form of a cluster of *m*/*z* values. Theoretical models of these ion clusters were in good agreement with those obtained experimentally. Ions attributable to the loss of halide ion from the molecular ion were also present, and in the iodo complexes, ion clusters at *m*/*z* 550 were observed due to the $[MoTp^*(NO)I]^+$ ion.

Electronic Spectra. The electronic spectra of the complexes all contain an intense band near the solvent cutoff (230 nm), which is also present in the spectrum of the Tp* ligand and so may be assigned to a Tp* ligand $\pi \rightarrow \pi^*$ transition. Among the other bands in the spectra of the chloro complexes, the band at *ca.* 280 nm varies very little in energy among the complexes and is too intense to be due to a d−d transition. A band in this position is also observed in the spectrum of $[Et_3NH][MoTp^*(NO)Cl_2]$, suggesting that it is due to a charge transfer within the {MoTp*(NO)Cl} moiety. The exact nature of this process has not been identified, but its energy lies in the appropriate range for a ligand-to-metal charge transfer (LMCT).[26] Furthermore, there are three ligands in the {MoTp*(NO)Cl} center with filled π orbitals (Tp^{*-}, NO^+, Cl^-) and the metal possesses unfilled d orbitals. Another intense band which is found between 335 and 415 nm can be attributed to $\pi \rightarrow \pi^*$ transitions within the polyene ligands, as it is also observed in the spectra of the free ligands, L-L. Finally, between 530 and 590 nm another band is observed which may be assigned to a metal-to-ligand charge transfer (MLCT) process on the basis of solvatochromism studies.[27]

The electronic spectra of the iodo complexes are comparable with those of their chloro analogues. The Tp* and polyene transitions described previously are present, as is the LMCT band. The position of this latter band is not significantly altered when the halide species present in the complex is changed from chloride to iodide. This suggests that the donor in this LMCT transition is not the halide, but either NO or Tp*. The position of the MLCT band in these complexes (535−605 nm) is similar, but not identical, to that found for their chloro analogues (530−590 nm).

EPR Spectra. The EPR spectra of the monometallic chloro complexes were obtained at X-band frequency in dichloromethane/toluene mixtures at room temperature and in frozen solution at 77 K. The spectra of the monometallic complexes are the same within the errors of measurement and contain signals with g_{iso} values of 1.974 (±0.001). The spectra also exhibit a hyperfine coupling pattern expected from a single molybdenum nucleus in natural abundance, with A_{iso} in the range (43−49) × 10^{-4} cm^{-1}. The g_{iso} value was calculated from the position of the strong central line ($I = 0$), and the A_{iso} value was calculated from the mean of the separations between the first two and the last two hyperfine lines. This eliminates any second-order effects.[28a] A representative example is shown in Figure 4a. The similarity of the nuclear magnetic moments of ^{95}Mo and ^{97}Mo (−0.913 and −0.933 μ_N, respectively) and the broadness of the lines mean that signals from complexes containing these two nuclei are not resolved. A second signal is visible in the spectrum of [MoTp*(NO)Cl(4,4′-bpy)] with g_{iso} = 1.940 and an A_{iso} of *ca*. 40 × 10^{-4} cm^{-1}. No sign of a second species is apparent in the cyclic voltammogram of this complex. A possible explanation for this second signal is the presence of a protonated form of the complex, *viz.* $[MoTp^*(NO)Cl(4,4'\text{-bpyH})]^+$. The most likely source of the proton is the dichloromethane used as the solvent since chlorohydrocarbons are potential Brønsted acids. Also we have previously found that this solvent can act as a source of chloride ion leading to the formation of [MoTp*(NO)Cl(mentholate)] from [MoTp*(NO)I-(mentholate)].[29] The EPR spectrum of $[MoTp^*(NO)Cl(4,4'\text{-bpyMe})]^+$ should be similar to that of $[MoTp^*(NO)Cl(4,4'\text{-bpyH})]^+$, but attempts to synthesize the N-methylated derivative of [MoTp*(NO)Cl(4,4′-bpy)], by reacting it with MeI, failed to provide a pure product. The EPR spectra of frozen solutions of the monometallic chloro complexes, at X-band frequency, were consistent with axial EPR symmetry. The anisotropic spin-Hamiltonian parameters, obtained by spectrum simulation,[28b] were in the ranges $g_{\|}$ 1.925−1.936, $g_{\perp}$ 2.004−1.997, $A_{\|}$ (68−70) × 10^{-4} cm^{-1}, and $A_{\perp}$ 33−35 cm^{-1}, and a representative spectrum is shown in Figure 4b.

The solution EPR spectra of the bimetallic chloro complexes are again very similar to each other and are characterized by g_{iso} values of 1.974 (±0.001) and A_{iso} in the range (44−48) × 10^{-4} cm^{-1}. A representative spectrum is shown in Figure 4c. The components expected from a bimetallic system with two equivalent molybdenum atoms in natural abundance, and each with formally one unpaired electron, are the following: a strong central line ($I_1 = I_2 = 0$), relative intensity = 1; 6 hyperfine lines ($I_1 = 0$, $I_2 = {}^5/_2$ plus $I_1 = {}^5/_2$, $I_2 = 0$), each with relative intensity 0.112; 11 hyperfine lines ($I_1 = I_2 = {}^5/_2$), relative intensities 0.0031, 0.0063, 0.0094, 0.0126, 0.0157, 0.0189, 0.0157, 0.0126, 0.0095, 0.0063, and 0.0031.[28a] In addition, the hyperfine splitting *observed* in the experimental spectrum should be half that for the corresponding monometallic centers. The experimental spectra are consistent with both of these expectations. The isotropic EPR spectra of these bimetallic complexes are characterized by the spin-Hamiltonian parameters g_{iso} in the range 1.974 ± 0.001 and A_{iso}, *for each metal center*, in the range (44−48) × 10^{-4} cm^{-1}. These parameters were obtained directly from the spectra as described above for the monometallic complexes. The spectra are also consistent with the exchange integral, *J*, *vide infra*, being large compared to the hyperfine interaction, A_{iso}.[30] However, this merely places a lower limit on $|J|$ of about 0.05 cm^{-1} and cannot confirm the much larger

(25) (a) Briggs, T. N.; Colquhoun, H.; El Murr, N.; Jones, C. J.; McCleverty, J. A.; Neaves, B. D.; Adams, H.; Bailey, N. A. *J. Chem. Soc., Dalton Trans.* **l985**, l249−1254.
(26) Shriver, D. F.; Atkins, P. W.; Langford, C. H. In *Inorganic Chemistry;* Oxford University Press: Oxford, U.K., 1990; p 446.
(27) Thomas, J. A.; Hutchings, M. G.; Jones, C. J.; McCleverty, J. A. Unpublished results.
(28) (a) Mabbs, F. E.; Collison, D. *Electron Paramagnetic Resonance of d-Transition Metal Compounds*; Elsevier: Amsterdam, 1992; pp 88−94. (b) *Ibid.* pp 223−273.
(29) Wlodarczyk., A; Kurek, S. S.; Foulon, D.-J.; Hamor, T. A.; McCleverty, J. A. *J. Chem. Soc., Dalton Trans.* **1992**, 981−987.
(30) (a) Reitz, D. C.; Weissmann, S. I. *J. Chem. Phys.* **1960**, *33*, 700−704. (b) Luckhurst, G. R. *Mol. Phys.* **1966**, *10*, 543−550. (c) Glarum, S. H.; Marshall, J. H. *J. Chem. Phys.* ***1967***, *47*, 1374−1378. (d) Hudson, A.; Luckhurst, G. R. *Chem. Rev.* **1969**, *69*, 191−225. (e) Atherton N. M. *Electron Spin Resonance, Theory and Applications*; Ellis Horwood: Chichester, U.K. 1973; p 182.

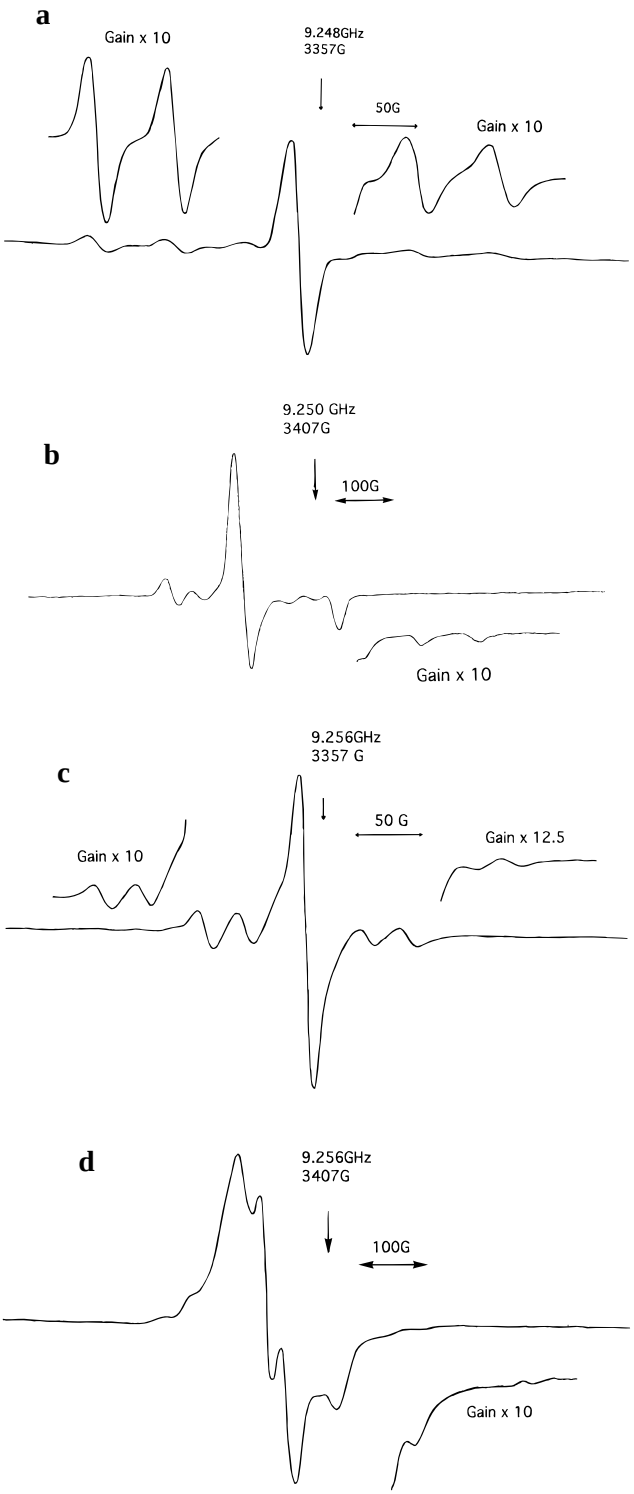

Figure 4. Typical examples of EPR spectra of the new complexes: (a) the 300 K solution spectrum of **12**, modulation amplitude 10 G, microwave power 20 mW, scan range 400 G, receiver gain 50; (b) the 77 K frozen solution spectrum of **12**, modulation amplitude 10 G, microwave power 20 mW, scan range 800 G, receiver gain 400; (c) the 300 K solution spectrum of **13**, modulation amplitude 10 G, microwave power 10 mW, scan range 400 G, receiver gain 100; (d) the 77 K frozen solution spectrum of **13**, modulation amplitude 10 G, microwave power 20 mW, scan range 800 G, receiver gain 800.

interaction indicated by the magnetic susceptibility measurements, *vide infra*.

The frozen solution spectra of the bimetallic complexes, see Figure 4d for a typical example, were less well resolved compared to those of the monomers, and we have found no evidence of resonances outside the magnetic field range shown.

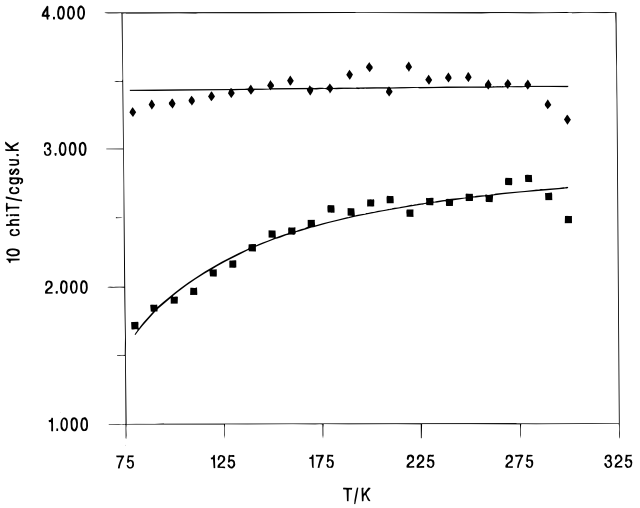

Figure 5. Variation of χT with temperature for the two complexes **9** (♦) and **10** (■). The lines are for Curie-law behavior (**9**) and the fitted Bleaney−Bowers' equation (**10**) (see text).

This behavior is consistent with the spectra arising from a spin triplet state (*cf.* the magnetic susceptibility, *vide infra*) with a small ($\ll h\nu$) zero-field splitting.

The lack of any observed hyperfine coupling to ligand nuclei is indicative of a ground state which is predominantly metal in character. In the monometallic complexes the $g_{||}$ values are less than the free electron value of 2.0023. This pattern of g values is consistent with the admixture into the singly occupied molecular orbital (SOMO) ground state, *via* spin−orbit coupling, of excited states arising from the SOMO to unoccupied molecular orbital excitation of the single electron.[31] The EPR parameters of the monometallic complexes described here are similar to those of $[MoTp^*(NO)(py)_2]^+$. In this latter complex a combination of the electronic absorption spectrum and the EPR parameters was used to assign the systems as tetragonally distorted octahedra with a d_{xy} ground state orbital.[22] A similar model was proposed earlier to describe the bonding in the d^5 chromium nitrosyl complex [Cr(tpp)(NO)] ($tppH_2$ = tetraphenylporphyrin), the EPR spectrum of which contained a signal with $g_{iso} = 1.993$.[32]

Magnetic Measurements. In order to determine whether the polyene chain in these complexes could support long range magnetic interactions, the magnetic susceptibility of **10** was determined over the temperature range 80−300 K. At room temperature the effective magnetic moment of **10** is 1.41 μ_B, well below the free spin value for a $S = {}^1/_2$ system and of the values for the related monometallic 17-electron complexes [MoTp*(NO)I(L)] (L = pyridine, 1.8; isoquinoline, 1.7; phenanthridine, 2.9 μ_B).[24] This value reduces to 1.17 μ_B at 80 K, a behavior that might be expected as a result of strong spin−orbit coupling or of antiferromagnetic exchange. As spin−orbit coupling effects are predicted to be important in the second-row transition series[33] (for Mo^I the spin−orbit coupling constant $\lambda = 672$ cm^{-1}),[34] the magnetic properties of the corresponding monometallic complex **9** were investigated. This complex obeys the Curie law quite closely, as shown in Figure 5, with a magnetic moment (*ca.* 1.71 μ_B) that is similar to [MoTp*(NO)I(L)][24] and mononuclear Mo^V species.[35] We conclude that the

(31) Stone, A. J. *Mol. Phys.* **1964**, *7*, 311−316.
(32) Wayland, B. B.; Olson, L. W.; Siddiqui, Z. U. *J. Am. Chem. Soc.* **1976**, *98*, 94−98.
(33) Mabbs, F. E.; Machin, D. J. In *Magnetism of Transition Metal Complexes;* Chapman and Hall: London, 1973; Chapter 7.
(34) Goodman, B. A.; Raynor, J. B. *Adv. Inorg. Chem. Radiochem.* **1970**, *13*, 135−362.

low magnetic moments of the dinuclear complex **10** and its temperature dependence are the consequences of magnetic exchange.

The variation of magnetic susceptibility of **10** with temperature is in accord with this conclusion. As Figure 5 shows, the data closely obey the Bleaney−Bowers' equation[36] (eq 2), with the best fit corresponding to $g = 1.80$ and $-2J = 82$ cm^{-1}.

$$\chi = (2Ng^2\mu_B{}^2/3kT)\{1 + (^1/_3)\exp(-2J/kT)\}^{-1} \qquad (2)$$

This low value of g accords with the predictions of spin−orbit effects. If g is forced to take higher values, the exchange interaction constant correspondingly becomes increasingly negative with significantly poorer fit to eq 2; $-2J = 98$ cm^{-1} for $g = 1.88$ (the value determined from the high-temperature limiting slope of the Curie−Weiss law plot for **10**), and $-2J = 115$ cm^{-1} for $g = 1.97$ (the value of g from the EPR study of **10**). In any case, the magnetic behavior of **10** displays a substantial antiferromagnetic exchange, which, if it is intramolecular, remarkably operates over a distance of more than 2 nm.

A mechanism for superexchange over such long distances in these molecules may be proposed on the basis of the crystal structure of **10** (*vide infra*). This shows that the plane of the pyridyl ring of the polyene ligand is inclined at *ca.* 45° to the rest of the ligands in the metal coordination spheres, as found in the {$Ru^{II}(NH_3)_5$(pyridyl)} unit, where the pyridyl ring also shows a 45° torsion angle.[37] In the model illustrated in Figure 6a, the d_{yz} and d_{xz} orbitals would be stabilized by interaction with the π* orbitals of the NO ligand, leaving d_{xy} as the higher energy SOMO as shown in Figure 6b. In accord with this model, the EPR spectra of [MoTp*(NO)(py)$_2$]$^+$ and **9** are consistent with axial symmetry associated with a tetragonally distorted octahedral coordination geometry at Mo.[22] Molecular orbital calculations on the free bipyridyl ligands using the AM1 MO method of the MOPAC package[38] indicate that, in the region of the Mo termini, the LUMO and HOMO of the free ligands have the form shown in Figure 6c. Thus overlap is possible between the d_{xy} SOMO and the HOMO of the bridging ligand (Figure 6d), providing a pathway for magnetic exchange. With an even number of p orbitals linking the pyridyl rings, the bridging ligand bpot has an extended occupied molecular orbital suitably aligned to mediate exchange between the magnetic orbitals of the Mo centers. That no pathway for magnetic exchange can be recognized between magnetic centers in different molecules (minimum intermolecular Mo−Mo 8.883 Å), and that antiferromagnetic interactions are not apparent in the related monometallic complexes [MoTp*(NO)I(L)][24] and **9**, leads us to conclude that the interaction is indeed intramolecular.

Electrochemistry. Electrochemical measurements were made using cyclic voltammetry and the Condecon 310 system, which allows information on the mechanism and kinetics of electrode processes to be obtained through the use of convolutions, kinetic convolutions, and deconvolutions.[39] Each monometallic chloro complex displayed a one-electron reduction process and a one-electron oxidation process (Table 3). The potentials for the oxidations were similar for all the complexes, and in selected examples of the bipyridyl polyene complexes, these were analyzed using the kinetic convolution facility of the Condecon package. These studies revealed slightly limited chemical reversibility, with some decomposition of the oxidation products taking place. However, electron transfer rates were generally fast, showing electrochemical reversibility.

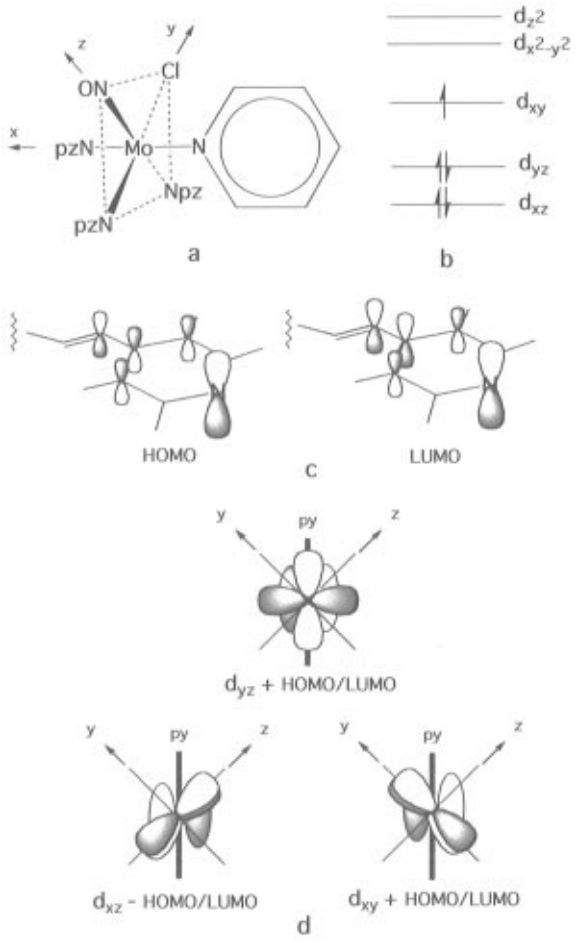

Figure 6. A possible model for the antiferromagnetic exchange observed in **10**: (a) the geometric arrangement of the {MoTp*(NO)-Cl(pyridyl)} moiety; (b) proposed energy order for the Mo d orbitals; (c) the form of the HOMO and LUMO of the bipyridyl polyenes within the pyridyl moiety; (d) diagrams illustrating the overlap of the filled Mo d orbitals with the HOMO or LUMO of the bipyridyl polyene ligand.

In order to establish the electron transfer characteristics of the reduction process in the monometallic complexes, plots were made of current against (scan rate)$^{-1/2}$ for each wave. All the plots deviated from linearity at fast scan rates. This is probably caused by a combination of slow electron transfer and slight decomposition. Comparison of the reduction potentials of the monometallic chloro complexes shows that, with the exception of bpa, the reductions of the bipyridyl complexes are all at least 300 mV more anodic than that of the pyridine complex [MoTp*-(NO)Cl(py)]. The AM1 MO calculations on the free ligands (Table 4) show that the π*-acceptor orbitals in the bipyridyls (excepting bpa) are between 0.9 and 1.3 eV lower in energy than in pyridine itself.[38,40] Thus it appears that the π*-acceptor ability of the bipyridyl ligand has a significant effect on the reduction potential of its monometallic complex.

The bimetallic chloro complexes generally showed two reduction processes (Figure 7) along with one oxidation process.

(35) Boyd, I. W.; Dance, I. G.; Murray, K. S.; and Wedd, A. G. *Aust. J. Chem.* **1978**, *31*, 279−284.
(36) Bleaney, B.; Bowers, K. D. *Proc. R. Soc. London* **1952**, *A214*, 451−465.
(37) Woitellier, S.; Launay, J. P.; Joachim, C. *Chem. Phys.* **1989**, *131*, 481−488.
(38) Dewar, M. J. S.; Zoebisch, E. G.; Healy E. F.;d Stewart, J. *J. Am. Chem. Soc.* **1985**, *107*, 3902−3909. QCPE Program 455 Version 6.0, Department of Chemistry, Indiana University, Bloomington, IN.
(39) (a) Bard, A. J.; Faulkner, L. R. In *Electrochemical Methods. Fundamentals and Applications;* Wiley: New York, 1980. (b) Imbeau, J. C.; Saveant, J. M. *Electroanal. Intrafacial Chem.* **1973**, *44*, 169−172.
(40) Petke, J. D.; Whitten, J. L.; Ryan, J. A. *J. Chem. Phys.* **1968**, *48*, 953.

Table 3. Electrochemical Data

	oxidation[a]		reduction[a]					
compound	E_f(ox)/V (ΔE_p/mV)	k_s/s^{-1} [b] {E_f(ox)}	$E_f(1)$/V (ΔE_p/mV)	$E_f(2)$/V (ΔE_p/mV)	ΔE_f/mV[c]	k_s/s^{-1} [b] {$E_f(1)$} {$E_f(2)$}	$\log_{10} K_c$[d]
[MoTp*(NO)Clpy]	+0.043 (95)		−2.005 (95)				
1	+0.108 (90)		−1.695 (90)				
2	+0.010 (85)		−1.408 (80)	−2.173 (85)	765		13.0
3	+0.035 (90)		−1.648 (85)				
4	+0.083 (115)		−1.453 (130)	−2.035 (130)	582		9.9
5	+0.026 (90)	0.33	−1.640 (110)				
6	+0.040 (90)	0.16	−1.480 (90)	−1.870 (90)	390		6.6
7	+0.025 (85)	0.17	−1.650 (110)				
8	+0.035 (85)	0.15	−1.510 (85)	−1.750 (90)	240		4.1
9	+0.025 (85)	0.20	−1.635 (90)				
10	+0.055 (80)	0.18	−1.525 *e*	−1.625 *e*	105[f]		1.8
11	+0.045 (65)	0.10	−1.060 (60)		(40)[g]		(4)[g]
12	+0.100 (80)		−1.918 (95)				
13	+0.115 (120)		−1.850 (120)	−2.055 (100)	205		3.5
14	+0.045 (100)		−2.033 (95)				
15	+0.080 (95)		−2.000 *e*	−2.105 *e*	105[f]		1.8
16	+0.140 (120)		−1.620 (170)			0.90	
17	+0.131 (75)		−1.375 (100)	−2.060 (120)	685	0.10 (1) 0.12 (2)	11.6
18	+0.118 (75)		−1.570 (130)			0.32	
19	+0.123 (90)		−1.380 (120)	−1.945 (110)	565	<0.1 (1) <0.1 (2)	9.6
20	+0.100 (85)		−1.585 (120)			0.40	
21	+0.120 (110)		−1.430 (130)	−1.845 (150)	415	0.20 (1) 0.60 (2)	7.0
22	+0.110 (110)		−1.595 (120)			0.32	
23	+0.110 (120)		−1.455 (150)	−1.720 (150)	265	<0.1 (1) <0.1 (2)	4.5
24	+0.090 (75)		−1.585 (90)			0.23	
25	+0.110 (80)		−1.480	−1.615	135[f]	*e*	2.3

[a] Electrochemical measurements made in a 0.2 M Bu_4NBF_4 solution in dichloromethane and are referenced to ferrocene used as an internal reference at a scan rate of 500 mV s^{-1}; under these conditions the convolution transform I_1/E of the ferrocene couple (E_f = 0.560 V vs SCE) showed an overlay of forward and reverse sweeps. Estimated errors: formal electrode potential, E_f ±5 mV; anodic/cathodic peak separation, ΔE_p ±5 mV. [b] Rate constants for the specified electron transfer determined from the kinetic convolution using the Condecon 310 software. [c] Difference between the two reduction potentials $\Delta E_f = [E_f(1) - E_f(2)]$; estimated error in ΔE_f ±5 mV. [d] Calculated from $\log_{10} K_c = \Delta E_f/59$. [e] Value not resolved due to overlap of waves. [f] Data obtained by differential pulse voltammetry.[9] [g] Estimated experimental value, not significantly different from theoretical value for noninteracting metal centers.

Table 4. HOMO and LUMO Energies for Bipyridyl Polyenes and Related Compounds

ligand	py	bpa	4,4′-bpy	bpe	bpbd	bpht	bpot	dmbpdp
LUMO energy (eV)	0.138	0.058	−0.776	−0.901	−1.080	−1.158	−1.210	−1.167
HOMO energy (eV)	−9.932	−10.015	−9.919	−9.377	−8.926	−8.652	−8.456	−8.216

However, in the cases of **10** and **25** the two reduction waves were not fully resolved by cyclic voltammetry, and in **11** only a single reduction wave was observed. Studies of **2** using the Condecon software package showed that the oxidation wave of the chloro complexes is irreversible, the oxidation product undergoing a chemical decomposition with a rate constant of about 1.0 s^{-1}. The two reduction waves of the bimetallic chloro complexes were found to be quasi-reversible, displaying slow

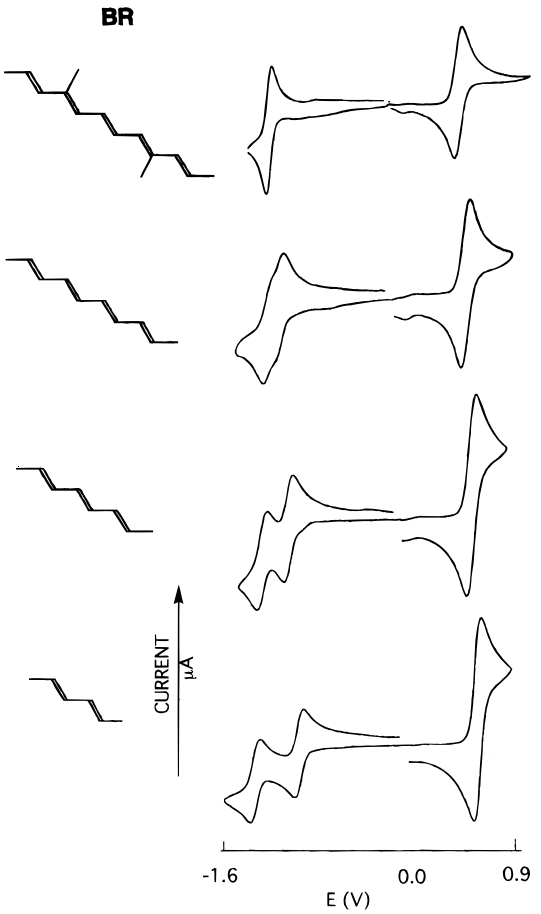

Figure 7. The cyclic volammograms of **11**, **10**, **8**, and **6**: [MoTp*-(NO)Cl(NC_5H_4)}$_2$(BR)], BR = bridging ligand.

electron transfer. Analysis of selected examples using convolutions indicated that the reduction products were stable with $k_f \leq 0.1\ s^{-1}$. Logarithmic plots showed that each of the two reductions, where resolved, involved one electron whereas the oxidation process involved two electrons. The free bipyridyl polyene ligands are themselves electrochemically active, but they show irreversible waves at more cathodic values ($E_f = -2.00$ to -2.36 V vs Fc/Fc^+) than those observed for these complexes. They also exhibit a smaller separation between their reduction potentials; the two irreversible reduction waves of the bpbd ligand, for example, are separated by 260 mV[41] compared to 390 mV in the bimetallic complex **6**. This suggests that the reduction waves for [{MoTp*(NO)Cl}$_x$$NC_5H_4$$(CHCH)_n$$C_5H_4N$] cannot be attributed to purely ligand-centered redox processes, but rather must contain substantial metal character.

Although the electrochemistry of the iodo complexes was similar to that of their chloro counterparts, there were some notable differences (Table 3). The oxidation potentials for all the iodo complexes showed an anodic shift of about 50 mV compared to their chloro analogues and appeared to depend upon the nature of the ligand. Analysis using convolutions, kinetic convolutions, and deconvolutions showed that all these oxidations involve fast electron transfer, and unlike the case with the chloro complexes, they were essentially chemically reversible with $k_f \leq 0.1\ s^{-1}$. This contrast in properties is particularly clear in the 4,4′-bpy complexes. The chloro complexes display chemical irreversibility toward oxidation, with a k_f value of about $1.0\ s^{-1}$, while for the iodide complex k_f is only about $0.05\ s^{-1}$. The reduction potentials of [{MoTp*(NO)I}$_x${$NC_5H_4$$(CHCH)_n$-$C_5H_4N$}] also show an anodic shift compared to the chloro

(41) Horner, M.; Hunig, S.; Putter, H. *Electrochim. Acta* **1982**, *27*, 205.

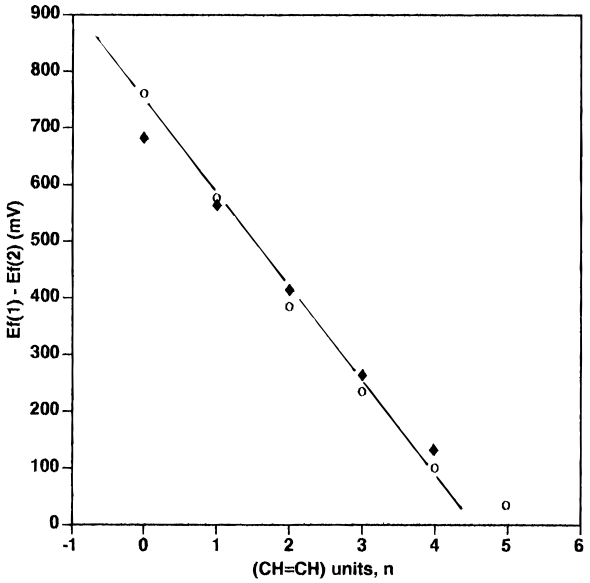

Figure 8. A plot of the difference between the first and second reduction potentials {$E_f(1) - E_f(2)$} of the bimetallic complexes **2**, **4**, **6**, **8**, **10**, **11**, **17**, **19**, **21**, **23**, and **25** against the number of ethen-diyl groups, *n*, in the polyene chain. The chloro complexes are denoted by open symbols (○) and the iodo complexes by closed (♦) symbols. The line is based on the best fit for **2**, **4**, **6**, **8**, and **10** and is given by {$E_f(1) - E_f(2)$} = $749 - 166n$; $r^2 = 0.9946$.

complexes, and while two reduction potentials were again observed, values of ΔE_f were different, being of a lower magnitude for the complexes with shorter ligand bridges and larger in magnitude for the more extended bridges.

These reduction processes of the iodo complexes did not display complete chemical reversibility, and some of the electron transfer processes were quasi-reversible. Therefore, detailed analysis of the reductions was carried out using the Condecon package. In particular, the monometallic complexes show limited chemical reversibility, and some show quasi-reversible electron transfers. The relative anodic shift in the redox chemistry of all the iodo complexes indicates a lowered electron density in the {MoTp*(NO)I} metal center as compared to that of the chloro complexes. This is in accord with the observed shifts of the ν_{max}(NO) in the IR spectra of the complexes.

The separation between the two reduction potentials, ΔE_f, of the bimetallic complexes was found to vary with polyene chain length, and a plot of ΔE_f against the number of {HC═CH} units, *n*, in the polyene chain for the chloro complexes (Figure 8) was linear over the range $n = 0-4$. Each increment in polyene chain length results in an almost monotonic decrease in ΔE_f of *ca*. 166 mV until, for **11**, the value of ΔE_f is experimentally indistinguishable from the statistical limit of $\Delta E_f = 36$ mV for two equivalent noninteracting redox centers. Similar behavior is found for the bimetallic iodo complexes. The value of ΔE_f correlates well with the calculated[38] energies (Table 4) of both the HOMO and LUMO in the bipyridyl polyene bridge, as well as with the HOMO−LUMO energy gap. However, since all these quantities correlate well with the polyene chain length, it is not surprising that they also correlate with ΔE_f.

Reimers and Hush have proposed[8b] an empirical model (eq 3) to describe the variation in the electrostatic interaction between two metal centers in a bimetallic complex, as indicated by ln K_c, with the metal−metal distance, r_{MM}. The series of

$$K_c = 4 \exp(1/\epsilon r_{MM} kT) \qquad (3)$$

cationic ruthenium bipyridyl polyene complexes, [{$(NH_3)_5$-

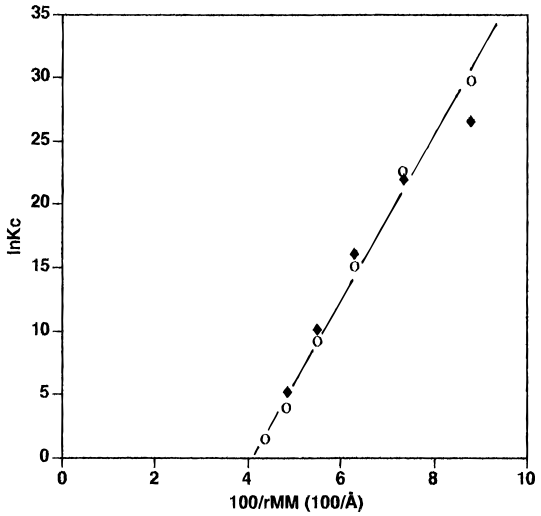

Figure 9. A plot of ln K_c against the reciprocal of the estimated metal−metal distance, r_{MM}. The line is given by ln $K_c = 613/r_{MM} + 24$; $r^2 = 0.9763$. The chloro complexes are denoted by open symbols (○) and the iodo complexes by closed (♦) symbols.

$Ru\}_2NC_5H_4(CHCH)_nC_5H_4N]^{4+}$ ($n = 0-4$), gives a linear plot of ln K_c vs $1/r_{MM}$ with an intercept at ln K_c = ln 4 for $1/r_{MM} = 0$ as predicted by the model.[42] In contrast, a similar plot for the molybdenum bipyridyl polyene complexes (Figure 9) falls steeply to reach ln K_c = ln 4 at $1/r_{MM} = 0.041$ Å^{-1} ($r_{MM} = 24.4$ Å). Thus, it seems that this electrostatic model does not apply to the molybdenum mononitrosyl systems described here. This marked difference in behavior reflects the substantial chemical differences between these two systems. In the series of cationic ruthenium complexes, the comproportionation equilibrium involves anodic couples which are essentially metal based and may be well separated from ligand redox couples. In the neutral molybdenum complexes, the couples are at cathodic potentials and would appear to involve significant ligand character as judged by the difference in potentials between the monometallic bipyridyl and pyridine complexes described earlier. Furthermore, the K_c values for the ruthenium complexes fall in the range 4−20 while for the molybdenum complexes the range is from 4 to 10^{13}, based on the relationship log $K_c = \Delta E_f$ /59 mV. However, this relationship is only valid if the standard potentials of the two redox couples are equal. While this may be the case in symmetrical bimetallic compounds where independant metal-centered redox couples are present, it may not be true of the molydenum complexes described here. The spectroelectrochemical studies (*vide infra*) suggest that the LUMO of the oxidized isovalent molybdenum complexes contains significant bipyridyl polyene character. Thus, the assumption that the standard potentials of the two redox couples are effectively equal may not apply, and ΔE_f may not be a good indicator of K_c. If this is so, it could account for the failure of the plot of ln K_c against $1/r_{MM}$ to agree with the Reimers and Hush model.

When the monometallic and bimetallic species are compared, it is found that the first reduction of the bimetallic complex is less cathodic than the reduction of its monometallic counterpart. This suggests that the electron density of the metal centers in the bimetallic complex is lower than that in the monometallic complex, and indeed, similar observations have been made on other complexes containing the {MoTp*(NO)Cl} metal center and pyridyl-based ligands.[43,44] Further evidence for this conclusion is found in the IR spectra of the complexes. All the monometallic species show ν_{max}(NO) values which are lower than the values for the corresponding bimetallic species, again indicating a higher electron density at the metal center in the monometallic complexes. One explanation for these findings is that mixing the electron-accepting, π^* LUMO of the polyene ligand with two metal orbitals produces greater stabilization than mixing with only one. Thus, the LUMO is relatively lower in energy in the bimetallic complexes. If this is the case, since the HOMO of the complexes appears relatively insensitive to the nature of the bipyridyl ligand (*vide infra*), the electronic spectra of the bimetallic complexes should show a bathochromic shift in their MLCT bands compared to those of the corresponding monometallic complexes. In fact, a shift of this kind is seen in the lowest energy band of the electronic spectra. A plot of the difference in energy between the lowest energy electronic transitions of the mono- and bimetallic complexes against the difference in their first reduction potentials is shown in Figure 10. Although subject to some scatter, this plot does reveal a general correlation between the reduction in energy of the MLCT and the anodic shift of the first reduction potential on going from the mono- to the bimetallic system.

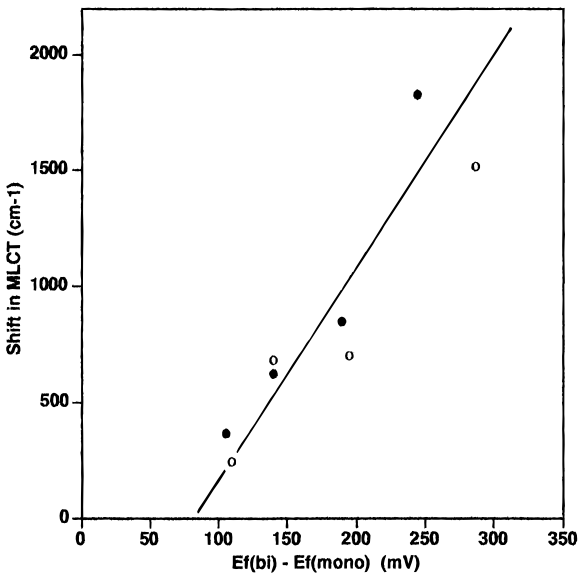

Figure 10. A plot of the shift in energy of the MLCT band between the monometallic complexes **1**, **3**, **7**, **9**, **16**, **18**, **22**, and **24** and their bimetallic counterparts **2**, **4**, **8**, **10**, **17**, **19**, **23**, and **25** against the corresponding difference in first reduction potentials {E_f(mono) − E_f(bi)}. The chloro complexes are denoted by open symbols (○) and the iodo complexes by closed (●) symbols. The line is given by shift in MLCT = 7.676{E_f(mono) − E_f(bi)} − 490; $r^2 = 0.8305$.

The difference between the first reduction potentials of the mono- and bimetallic complexes may also be correlated with the magnitude of the separation between the first and second reduction potentials of the bimetallic complexes. A plot of this type is shown in Figure 11 and reveals quite a good linear correlation for the polyenes with $n = 1-4$. However, the points for the 4,4′-bpy complexes did not fall close to this line. Although the 4,4′-bpy complexes are considered to be members of the series of bipyridyl polyene complexes, they differ in one important respect from the other members of the series. The torsion angles between the two pyridyl rings in the bridging ligand will generally be small for the ligands with $n = 1$ or more, whereas when $n = 0$ twisting about the pyridyl−pyridyl C−C bond can occur, giving rise to significant torsion angles.

(42) Ribou, A.-C.; Launay, J.-P.; Takahashi, K.; Takayasu, N.; Tarutani, S.; Spangler, C. W. *Inorg. Chem.* **1994**, *33*, 1325−1329.
(43) McWhinnie, S. L. W. Ph.D. Thesis, University of Birmingham, U.K., 1989.
(44) Das, A.; Maher, J. P.; McCleverty, J. A.; Navas-Badiola, J. A.; Ward, M. D. *J. Chem. Soc., Dalton Trans.* **1993**, 681−686.

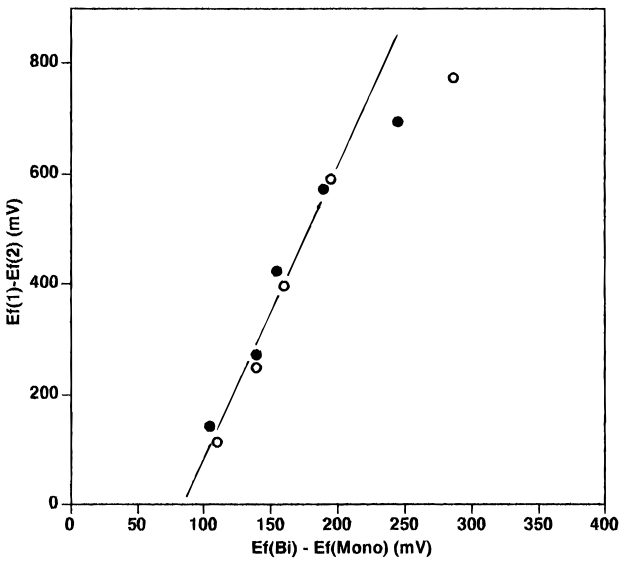

Figure 11. A plot of the difference between the first and second reduction potentials $\{E_f(1) - E_f(2)\}$ of the bimetallic complexes **2**, **4**, **6**, **8**, **10**, **17**, **19**, **21**, **23**, and **25** against the corresponding difference in first reduction potentials $\{E_f(\text{mono}) - E_f(\text{bi})\}$ of these bimetallic complexes and their monometallic counterparts **1**, **3**, **5**, **7**, **9**, **16**, **18**, **20**, **22**, and **24**. The chloro complexes are denoted by open symbols (○) and the iodo complexes by closed (●) symbols. The line is given by $\{E_f(1) - E_f(2)\} = 3.81\{E_f(\text{mono}) - E_f(\text{bi})\} - 244$; $r^2 = 0.9262$.

Indeed this bond in free 4,4′-bpy is strongly twisted and a free rotor in solution.[45] When bpy is incorporated into a metal complex, it can be either planar or nonplanar, and this can greatly influence the physical properties of its complexes.[46] Work by Woitellier *et al.* has demonstrated that $\pi-\pi^*$ coupling between metal centers is maximized in systems bridged by the planar conformer of 4,4′-bpy.[37] Other work has shown that, as the occupancy of the π^* orbital in such ligands increases, the inter-ring C−C bond takes on more double-bond character.[47] This forces the ligand to become more planar, and as the dihedral angle of the two rings is reduced, there is a corresponding lowering in the energy of the π^* orbital. This allows a better interaction between the metal and bridging ligand, thus lowering the electron density around the metal center and increasing the occupancy of the π^* orbital. In this context it is noteworthy that in the phenylpyridine complex $[MoTp^*(NO)(NC_5H_4\text{-}4\text{-}Ph)_2]^+$ torsion angles of 30 and 41° are found between the pyridyl and phenyl rings,[24] while the related complex $[MoTp^*(NO)Cl(NC_5H_4\text{-}4\text{-}Ph\text{-}4'\text{-}OMe)]$, in which a methoxy π-donor group is located in the para position on the phenyl ring, exhibits a torsion angle of only 5°.[48] Since the observed ΔE_f value for **2** does not deviate strongly from the line in Figure 8, it seems likely that the torsion angle in the 4,4′-bpy ligand is relatively small. Furthermore, work on {MoTp*(NO)Cl} complexes incorporating the nonplanar 3,3′-dimethyl-4,4′-bipyridine ligand reveals a ΔE_f of 350 mV for $[\{MoTp^*(NO)Cl\}_2(NC_5H_3\text{-}3\text{-}Me\text{-}4\text{-}(C_5H_3N\text{-}3'\text{-}Me)\}]$ compared to 765 mV in **2**.[44] In addition, the MLCT of the 3,3′-bpy complex is hypsochromically shifted by 80 nm (577 → 497 nm), indicating that the ligand acceptor orbital is at a higher energy than in the 4,4′-bpy derivative. These differences may be attributed to the presence of a much larger torsion angle between the pyridyl rings resulting from the steric effects of the methyl groups in 3,3′-dimethyl-4,4′-bipyridine. This will increase the LUMO energy of the bridging ligand and reduce any bridge-mediated intermetallic interaction compared to the 4,4′-bpy system. In the cases of **14** and **15**, where the pyridyl groups are linked by a saturated bridge, $\pi-\pi^*$ coupling effects are not possible, and this is reflected in the relatively small difference between the reduction potentials of these two compounds.

In contrast to the reduction data, the oxidation data show much less variation, and the oxidations of the bimetallic complexes show no detectable splitting. However, there is some further evidence to support the arguments presented above. All the monometallic complexes oxidize at a slightly less anodic potential than their corresponding bimetallic complexes, again suggesting that the electron density around the metal center in the former is greater than in the latter. The marked contrast in the sensitivity of the oxidation and reduction processes to the nature of the pyridyl ligand can be explained by considering the contribution of the metal center and the bridging ligand toward the HOMO and LUMO of the complex. Several groups have attempted to correlate the redox processes of metal complexes with charge transfer bands observed in their electronic spectra,[49] the HOMO being associated with oxidations and the LUMO with reductions. In the case of the bipyridyl complexes, the reduction potentials are dependent on the degree of saturation of the ligand, ranging from −2.033 V for the monometallic complex based on bipyridyl ethane to −1.635 V for **9**. This would suggest that the LUMO of these complexes contains significant ligand character. However, the oxidation potentials are much less sensitive to the nature of the ligand, suggesting that the HOMO of these complexes is much more metal based. This offers further evidence that the observed optical CT band must be a MLCT transition.

Lever *et al.* have derived a relationship between the optical transition energy of MLCT processes and electrochemical potentials.[50] The energy of an MLCT transition such as

$$\{M^{n+}L\} \rightarrow \{M^{(n+1)+}L^-\} \quad (4)$$

is estimated by taking the two electrochemical potentials for metal oxidation, $E[\{M^{(n+1)+}L\}/\{M^{n+}L\}]$, and ligand reduction, $E[\{M^{n+}L\}/\{M^{n+}L^-\}]$

$$E_{op}(\text{MLCT}) = E[\{M^{(n+1)+}L\}/\{M^{n+}L\}] - E[\{M^{n+}L\}/\{M^{n+}L^-\}] + [(\chi_i + \chi_o) - y] \quad (5)$$

where M and L represent the metal and ligand involved in the transition, χ_i and χ_o are the inner (vibrational) and outer (solvation) reorganization energies, and y is a correction factor required as the MLCT process involves a $\{M^{n+1}L\}/\{M^{(n+1)+}L^-\}$ transition, while it is only possible to measure the $\{M^{n+}L\}/\{M^{n+}L^-\}$ couple.

To investigate if such a correlation existed for $[MoTp^*(NO)Cl\{NC_5H_4(CHCH)_nC_5H_4N\}]$, values of E_{op}(MLCT) were plotted against the calculated values of $[E_f(\text{oxidation}) - E_f(\text{reduction})]$ (Figure 12). Points were not included for compounds **5**, **6**, and **20** since the MLCT band was not clearly resolved in their spectra. In the case of **14**, the band at 615 nm is insufficiently

(45) Emsley, J. W.; Stephenson, D. S.; Lindon, J. C.; Lunizzi, L.; Pulga, S. *J. Chem. Soc., Perkin Trans.* **1975**, *2*, 1541−1544.
(46) Chen, P.; Curry, M.; Meyer, T. J. *Inorg. Chem.* **1989**, *28*, 2271−2280.
(47) (a) Cooke, B. J.; Palmer, T. F. *Photochemistry* **1984**, *26*, 149−163. (b) Fujii, T.; Suzuki, S.; Komatsu, S. *Chem. Phys. Lett.* **1978**, *57*, 175−178.
(48) Das, A.; Jeffrey, J. C.; Maher, J. P.; McCleverty, J. A.; Schatz, E.; Ward, M. D.; Wollermann, G. *Inorg. Chem.* **1993**, *32*, 2145−2155.
(49) (a) Curtis, J. C.; Sullivan, B. P.; Meyer, T. J. *Inorg. Chem.* **1983**, *22*, 224−229. (b) Lever, A. B. P. In *Inorganic Electronic Spectroscopy*, 2nd ed.; Elsevier: The Netherlands, 1984; pp 778−779.
(50) Haga, M.-A.; Dodsworth, E. S.; Lever, A. B. P. *Inorg. Chem.* **1986**, *25*, 447−453.

Table 5. Spectroelectrochemistry Results

complex	solvent	λ_{max}/nm[a] (ϵ/dm^3 mol^{-1} cm^{-1})							
[L*Mo(NO)Cl(py)]	CH_2Cl_2	620 (150)	467 (1250)	409 (1540)					
[L*Mo(NO)Cl(py)]$^-$	CH_2Cl_2	804 (4390)	462 (1500)	399 (2700)					
[**1**]$^-$	CH_2Cl_2	811 (37 420)	470 (12 890)	388 (15 650)					
[**2**]$^-$	CH_2Cl_2	880 (31 740)	544 (13 430)	426 (10 560)	359 (6110)				
2	DMF	558 (4460)	355 (6810)						
[**2**]$^-$	DMF	870 (21 320)	547 (10 270)	432 (8260)	355 (6030)				
[**2**]$^{2-}$	DMF	1189 (24 780)	547 (7140)	493 (8150)	431 (9040)	353 (10 270)			
[**6**]$^-$	CH_2Cl_2	1086 (57 185)	952 (48 775)	781 (40 365)	699 (35 880)	563 (21 850)	506 (16 800)	270 sh	
[**8**]$^-$	CH_2Cl_2	1212 (97 300)	1020 (70 000)	917 (67 800)	793 (48 650)	724 (28 000)	595 (26 550)	534 (26 500)	277 sh
[**9**]$^-$	CH_2Cl_2	1111 (20 050)	909 (15 050)	763 (18 230)	625 (19 150)	571 (14 600)	510 (10 950)		
[**10**]$^-$	CH_2Cl_2	1282 (64 700)	1025 (70 580)	892 (64 750)	806 (63 750)	666 (49 000)	628 (57 000)	588 (39 300)	271 sh

[a] Spectra obtained in 0.4 M Bu_4NBF_4 solution of the solvent indicated at −20 °C.

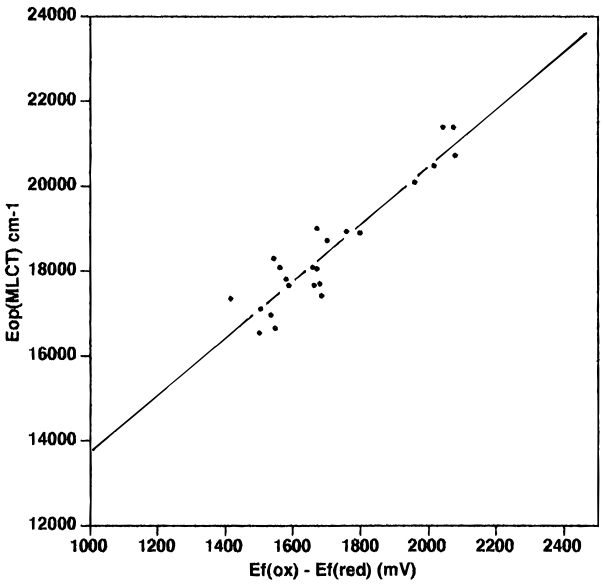

Figure 12. A plot of the energy of the MLCT band {E_{op}(MLCT)} against the difference between the oxidation and reduction potentials {E_f(ox) − E_f(red)} for the complexes **1**−**4**, **7**−**19**, **21**−**25,** and [MoTp*(NO)Cl(py)]. The line is given by E_{op}(MLCT) = 6.780{E_f(ox) − E_f(red)} + 6867; r^2 = 0.8726.

intense to be due to MLCT and the absorption at 482 nm was taken to be the MLCT band. Taken overall this plot showed a fair correlation, although there was some scatter in the data. This result is in accord with the proposal that the HOMOs of the complexes show a large metal character, while the LUMOs are more ligand in character.

Spectroelectrochemistry. In an attempt to obtain further information about the monoreduced form of the bimetallic complexes, the reductive electrolyses of [MoTp*(NO)Cl(py)], **1**, **2**, **6**, **8**, **9**, and **10** were carried out in dichloromethane, and the results are summarized in Table 5. By reduction of the bimetallic complexes to compounds which are formally mixed valence, the extent of metal−metal coupling might be assessed by analyzing any IVCT band present in the near-IR region of the electronic spectrum. The reduction of **1** appeared to be reversible at −20 °C as demonstrated by reversing the electrolysis while still monitoring the electronic spectra. The major change upon reduction of the 17-electron molybdenum species is the development of a charge transfer band at around 810 nm. The spectra of [Tp*Mo(NO)Cl(py)]$^-$ (Figure 13a) and [**1**]$^-$ are very similar in that they both show three transitions of similar energy in the region monitored (Table 5). However, the spec-

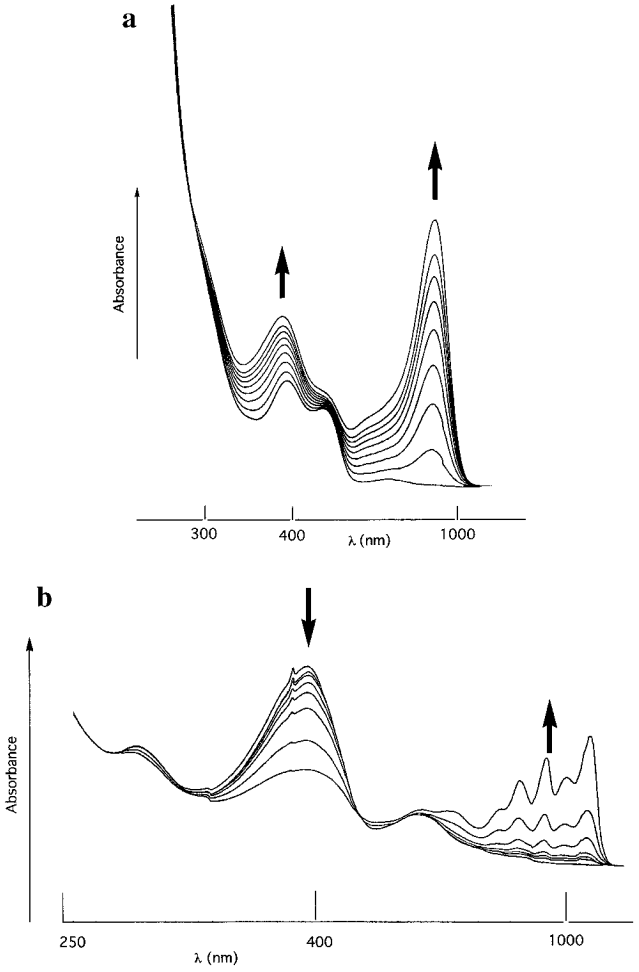

Figure 13. Examples of spectroelectrochemical traces for the first reductions of (a) [MoTp*(NO)Cl(py)] and (b) **2**.

trum of $[\mathbf{1}]^-$ is much more intense than that of [Tp*Mo(NO)Cl(py)]$^-$. Reductive electrolysis of **2** was carried out in dichloromethane and in dimethylformamide at −20 °C. It was found that the reduction was irreversible if carried out in dichloromethane at room temperature but was reversible in both solvents at −20 °C. In addition, the second reduction was carried out in dimethylformamide, also at −20 °C, but was found to be irreversible. As found for the monometallic species **1**, reduction of bimetallic **2** leads to the evolution of a low-energy charge transfer band, which moves to lower energy as the second electron is added. In an additional experiment, a more highly concentrated solution of **2** was electrolyzed and the near-IR spectrum was monitored to detect any low-intensity bands. A band was seen to evolve under the solvent overtone bands as the electrolysis proceeded. However, no maximum was observed for this band, although extrapolation indicates that the maximum would be at about 2860 nm.

The spectroelectrochemistry of the bimetallic polyene complexes **6**, **8**, **9**, and **10** showed that at −20 °C all the monoreduced products could be reversibly generated. Isosbestic points indicated that only two species were present in each reduction process. However, the second reduction of the bimetallic complexes proved to be irreversible. The monoreduced forms of all the complexes displayed similar characteristics, all the spectra displaying bands between 625 and 570 nm, and it seems likely that these are CT bands. Certainly they are at approximately the same energy as the MLCT in the neutral complexes (Table 5).

A particularly striking feature of these spectra is the development of intense bands at low energies (Table 5), an example being shown in Figure 13b. The structure and intensity of these bands are characteristic of polyene chromophores.[51] However, these transitions are at lower energy than would normally be expected. These observations are consistent with the LUMO of the neutral complex having significant ligand character. The reason for the bathochromic shift of the transitions is that the separation of the HOMO and the LUMO in the neutral molecule is much larger than the separation of the LUMO and the second lowest unoccupied orbital (SLUMO).[52] Thus, in the reduced species, the transition is a relatively lower energy process. If the reduced bimetallic complexes are mixed valence, then it is likely that they should show an IVCT band in the near-IR region. Unfortunately, this area is dominated by the aforementioned ligand bands so that no firm conclusions can be drawn on the nature of the monoreduced species.

Structural Studies. Selected geometric parameters of **10** are given in Table 6. The atom numbering scheme used is shown in Figure 3. The molecule is centrosymmetric, the mid-point of the C24−C24A bond coinciding with the crystallographic inversion center ($^1/_2$,$^1/_2$,$^1/_2$). The two molybdenum atoms are separated by 20.764(3) Å.

The coordination about molybdenum is essentially octahedral, with a maximum deviation from the ideal octahedral angle of 9.4° [angle N6−Mo−N8 = 170.6°] and mean deviation of 3.9°. Similar angular deviations are found in other complexes based on the {Mo(NO)Tp*} moiety where the other two bonds completing the octahedron are relatively long. Thus in the piperidine complex [Mo(NO)Tp*I(NHC$_5$H$_{10}$)],[23] Mo−N(piperidine) = 2.241(6) Å and the mean angular deviation from ideal octahedral is 4.3°, and in the pyridyl complex [Mo(NO)Tp*Cl(NC$_5$H$_4$C$_6$H$_4$OMe-4,4′)],[48] Mo−N(pyridyl) = 2.204(5) Å and the mean deviation is 4.4°. However, in the amido complexes [Mo(NO)Tp*I(NC$_4$H$_8$)],[23] Mo−N(pyrrolidine) = 1.937(5) Å, [{Mo(NO)Tp*Cl}$_2$(NC$_4$H$_8$N)],[53a] Mo−N(piperazin-1,4-diyl) = 1.942(6) Å, [Mo(NO)Tp*(NHC$_5$H$_4$N)$_2$],[53b] Mo−N(amido) = 1.987(3) and 1.990(3) Å, and [Mo(NO)Tp*(NHBu^n)$_2$],[53c] Mo−N(amido) = 1.945(19) and 1.935(20) Å, where the mean deviations are somewhat greater at 5.6, 5.6, 7.1, and 7.5°, respectively. An alternative electronic rationalization for this difference is that the former class of complexes and the present compound are 17-electron complexes, while the latter are 16-electron complexes. In favor of the steric distinction is the fact that the largest deviations from the ideal octahedron occur in the complexes containing *two* short bonds.

Table 6. Selected Geometric Parameters for **10**

Bond Lengths (Å) with Esd's in Parentheses			
Mo(1)−Cl(1)	2.415(6)	N(1)−O(1)	1.091(34)
Mo(1)−N(1)	1.896(23)	C(18)−C(21)	1.447(11)
Mo(1)−N(2)	2.208(7)	C(21)−C(22)	1.334(12)
Mo(1)−N(4)	2.186(7)	C(22)−C(23)	1.426(12)
Mo(1)−N(6)	2.153(6)	C(23)−C(24)	1.356(13)
Mo(1)−N(8)	2.196(6)	C(24)−C(24A)	1.449(17)

Selected Bond Angles (deg) with Esd's in Parentheses			
Cl(1)−Mo(1)−N(1)	92.8(3)	N(2)−Mo(1)−N(6)	85.9(3)
Cl(1)−Mo(1)−N(2)	89.4(2)	N(4)−Mo(1)−N(6)	83.9(2)
N(1)−Mo(1)−N(2)	177.0(4)	Cl(1)−Mo(1)−N(8)	93.7(2)
Cl(1)−Mo(1)−N(4)	173.1(2)	N(1)Mo(1)−N(8)	90.6(3)
N(1)−Mo(1)−N(4)	93.5(4)	N(2)−Mo(1)−N(8)	87.1(2)
N(2)−Mo(1)−N(4)	84.5(2)	N(4)−Mo(1)−N(8)	89.2(2)
Cl(1)−Mo(1)−N(6)	92.6(2)	N(6)−Mo(1)−N(8)	170.6(2)
N(1)−Mo(1)−N(6)	96.1(4)	Mo(1)−N(1)−O(1)	172.3(12)

The Mo−N(nitrosyl) bond length of 1.896(23) Å is rather long. Previous measurements of this bond in Mo(NO)Tp* complexes have generally resulted in significantly shorter lengths, 1.774(6),[23] 1.778(5),[23] 1.804(10),[53a] 1.751(3),[53b] 1.748(21),[53c] and 1.765(5)[29] Å. The N−O bond length at 1.091(34) Å is close to the range of values, 1.1−1.2 Å, in the literature.[23,29,53] The abnormal Mo−N bond length is presumably an artifact of the NO/Cl disorder discussed in the Experimental Section. The usual near linearity of this grouping has, nevertheless, been maintained, angle Mo−N−O = 172(1)°. A similar disorder has been observed[48] in the crystal structure of [Mo(NO)Tp*Cl(NC$_5$H$_4$C$_6$H$_4$OMe)].

The pyrazolyl rings are planar to well within the limits of experimental error. The interplanar angles are in the range 116−123°, with the smallest angle between the rings encompassing the relatively small nitrosyl ligand. The pyridyl ring is oriented in such a way as to be almost coplanar with the *trans* pyrazolyl ring (atoms N6, N7, and C12−C14), interplanar angle 7.0°, and almost equi-inclined to the other two pyrazolyl rings, interplanar angles 61.7 and 58.8°. The two symmetry-related pyridine rings are quite closely coplanar with the linking polyene chain, deviations ranging from 0.009 Å at the bonded atom, C21, to 0.29 Å at C21A, and the two rings are parallel to one another with interplanar separation of 0.30 Å. The polyene chain has the all-*trans* conformation with torsion angles (Table 7) deviating from the requirements of a planar structure by less than 5°. The formal double bonds average 1.345 Å, and the single bonds average 1.437 Å. Accepted values for pure double and single bonds in a system of trigonally hybridized carbon atoms are around 1.335 and 1.48 Å, so that some degree of electron delocalization occurs along the chain. The length of the C18−

(51) W. Kemp, W. In *Organic Spectroscopy;* Macmillan: London, 1979; p l54.
(52) Kaim, W. *Coord. Chem. Rev.* **1987**, *76*, 187−235.
(53) (a) AlObaidi, N.; Hamor, T. A.; Jones, C. J.; McCleverty, J. A.; Paxton, K. *J. Chem. Soc., Dalton Trans.* **1987**, 2653−2660. (b) AlObaidi, N.; Hamor, T. A.; Jones, C. J.; McCleverty, J. A.; Paxton, K. *J. Chem. Soc., Dalton Trans.* **1987**, 1063−1069. (c) AlObaidi, N.; Hamor, T. A.; Jones, C. J.; McCleverty, J. A.; Paxton, K. *J. Chem. Soc., Dalton Trans.* **1986**, 1525−1530.

Table 7. Selected Torsion Angles within the Polyene Chain

atoms	torsion angle (deg)[a]
C19−C18−C21−C22	0.7
C18−C21−C22−C23	179.2
C21−C22−C23−C24	−176.0
C23−C24−C24B−C23B	180.0

[a] Esd's approximately 1.5°.

C21 bond at 1.447(11) Å appears to allow the possibility that the pyridine ring is also involved in conjugation with the polyene chain.

In more quantitative terms, the "aromaticity constant", *A*, defined by Julg and Francois[54] as

$$A = 1 - K\sum(l_i - l')^2/nl'^2$$

for a system of alternate double and single bonds, where l' is the mean of the *n* bond lengths in the system, calculates to be 0.65. For a polyene chain, this value is a measure of the degree of electron delocalization and is broadly in agreement with the general conclusion that delocalization does occur to a modest extent. In this calculation we have taken *K* to be 297.5, so as to give an aromaticity (or delocalization) of 0 for bonds of lengths 1.316 and 1.47 Å.[55]

It has been proposed that the extent of bond length alternation in polyene-bridged donor−acceptor compounds may be used as an indicator of their potential nonlinear optical properties.[56] In octatetraene[57] and diphenyloctatetraene[58] the average difference between the alternating single and double carbon−carbon bonds of the polyene chain, $[r_{C-C}-r_{C=C}]$, is 0.11 Å compared to values of 0.02−0.05 Å in some donor−acceptor substituted polyene derivatives and essentially 0 in cyanine dyes.[59] In **10** a value of 0.092 Å is found for $[r_{C-C}-r_{C=C}]$ indicating that, in the isovalent ground state complex at least, complexation to the {MoTp*(NO)Cl} moiety is not strongly perturbing bonding in the polyene chain.

Conclusions

The series of redox active mono- and bimetallic bipyridyl polyene complexes described here show quite different behavior from their counterparts containing $\{Ru(NH_3)_5\}^{2+}$ termini. Their oxidation potentials are little affected by the nature of the pyridyl coligand, suggesting that the HOMOs of the new complexes are largely metal in character. In accord with this, the EPR data indicate that the electron in each SOMO is largely metal based. The large differences between the reduction potentials of the complexes and those of the free bipyridyl ligands suggest that the LUMOs of the complexes have substantial metal character. However, although at first sight the electrochemical data appear to be in accord with the complexes being reduced to mixed valence compounds with varying degrees of metal−metal interaction, the ΔE_f values for the bimetallic complexes cannot be converted to K_c values which are open to simple interpretation in terms of mixed metal valence states. That is, the the variation in ln K_c with $1/r_{MM}$, although linear, does not follow the model of Hush and Reimers.[8b] Furthermore, the spectroelectrochemical data do not provide evidence to support such a simple mixed metal valence model and suggest that the LUMO in the complexes also contains significant bridging ligand character. In the monoreduced complexes the new bands may more appropriately be interpreted as intraligand CT or MLCT transitions than as metal−metal CT processes. Thus, a simple metal-centered two-level model seems inappropriate to describe the electronic properties of the bimetallic complexes because of the presence of strong metal−bridging ligand interactions. One notable feature of the bimetallic complexes is the development of a strong low-energy absorbance in the monoreduced state. If this absorbance is ligand based and can be induced by excitation of the MLCT band, the bimetallic complexes could constitute an optical switch whereby excitation at one wavelength induces a large change in absorbance at another, longer, wavelength.

Acknowledgment. We are grateful to Dr. N. R. Armstrong for helpful comments and to SERC, Zeneca Specialties (J.A.T.), and The Royal Society (D.C.) for supporting this work.

Supporting Information Available: Full listings of H atom coordinates, bond distances and angles, and anisotropic thermal parameters and tables of elemental analyses, nitrosyl stretching frequencies, and electronic spectra (8 pages). Ordering information is given on any current masthead page.

IC950358+

(54) Julg, A.; Francois, P. *Theor. Chim. Acta* **1967**, *8*, 249−259.
(55) Allen, F. H.; Kennard, O.; Watson, D. G.; Brammer, L.; Orpen, A. G.; Taylor, R.; *J Chem. Soc., Perkin Trans. 2* **1987**, S1−S19.
(56) Marder, S. R.; Perry, J. W.; Tiemann, B. G.; Gorman, C. B.; Gilmour, S.; Biddle, S. L.; Bourhill, G. *J. Am. Chem. Soc.* **1993**, *115*, 2524−2526.
(57) Baughman, R. H.; Kohler, B. E.; Levy, I. J.; Spangler, C. *Synth. Met.* **1985**, *11*, 37−52.
(58) Drenth, W.; Wiebenga, E. H. *Acta Crystallogr.* **1955**, *8*, 755−760.
(59) (a) Groth, P. *Acta Chem. Scand. B* **1987**, *41*, 547−550. (b) Chentli-Bechikha, F.; Declercq, J. P.; Germain, G.; Meersshe, M. V. *Cryst. Struct. Commun.* **1977**, *6*, 421−424.